Influences on Post-Correction Nonuniformity of Infrared Focal Plane Arrays

by

Amory Wakefield

Submitted to the Department of Electrical Engineering and Computer Science
in partial fulfillment of the requirements for the degree of

Master of Engineering in Electrical Engineering and Computer Science

at the

MASSACHUSETTS INSTITUTE OF TECHNOLOGY

June 1997

Author .....
Department of Electrical Engineering and Computer Science
May 9, 1997

Certified by .....
Clifton G. Fonstad, Jr.
Professor of Electrical Engineering
Thesis Supervisor

Certified by .....
Donald L. Lee, Ph.D.
Staff Engineer, Lockheed Martin IR Imaging Systems
Thesis Supervisor

Accepted by .....
Arthur C. Smith
Chairman, Department Committee on Graduate Theses

Influences on Post-Correction Nonuniformity of Infrared Focal Plane Arrays

by

Amory Wakefield

Submitted to the Department of Electrical Engineering and Computer Science
on May 13, 1997, in partial fulfillment of the
requirements for the degree of
Master of Engineering in Electrical Engineering and Computer Science

Abstract

This thesis examines the influences on the post-correction nonuniformity of infrared focal plane arrays. Several possible contributors are enumerated and investigated. These fall into three major categories: testing, detector, and focal plane array characteristics. Extensive testing of long-wave, infrared focal planes arrays illuminated a few test procedures that were causing large amounts of post-correction nonuniformity. These were remedied and then focal plane parameters, particularly the silicon read-out integrated circuit, are indicated as dominating the results. Detector characteristics, though relevant to pre-correction response, are shown to have no correlation with large degrees of post-correction nonuniformity.

Thesis Supervisor: Clifton G. Fonstad, Jr.
Title: Professor of Electrical Engineering

Thesis Supervisor: Donald L. Lee, Ph.D.
Title: Staff Engineer, Lockheed Martin IR Imaging Systems

Acknowledgments

As with any large body of work, this thesis is not solely the work of an individual. Without the support, advice, and collaboration of many others, this work would never have been completed. I would like to extend my thanks to all who helped me, but specifically the following people:

Prof. Clif Fonstad and Dr. Don Lee, my advisors. This thesis would not be as clear, as focused, or as coherent without their time and effort to make it so.

Donald Grays, Joseph Czapski, and Kent Kuhler, my fellow FPA testers. Their experience and patience saved me hours in the test lab, while their good humor made the hours there much more bearable.

Nancy Hartle, Pete Campoli, Frank Jaworski, Kevin Maschhoff, and Jim Stobie all provided me with valuable technical guidance and support.

Doug Brown, Rosanne Tinkler, and Jill Wittels, who made my lunch, coffee, and stress breaks energizing, while reminding me to keep everything in proper perspective.

Josie, who ungrudgingly put up with my poor housekeeping, constant griping, and perpetual stressing.

Mike, who called upon his own thesis–writing experiences to illustrate that it does end, you do finish, and pain and panic are part of the process.

Paul, whose faith, understanding, and strength kept me together through the whole thing.

Finally, my family. Without them, I would not be doing this work at all and their much–needed moral support has helped me throughout my time at MIT.

Contents

List of Figures

List of Tables

Chapter 1

Introduction

1.1 Infrared Focal Plane Arrays

This thesis examines aspects of the performance of an infrared (IR) focal plane array (FPA) related to its response uniformity and linearity. An IRFPA is a key component in an IR imaging system. Infrared imaging systems are used in a wide variety of applications to view electromagnetic radiation in the 1 micron to 1 millimeter range, usually considered the "heat" radiating from an object. The following sections describe what composes an IRFPA.

1.1.1 Overview

The majority of FPAs are "hybrids" composed of two main parts, a detector array and a read–out integrated circuit (ROIC). The majority of infrared detector arrays utilized in these hybrids are fabricated using either mercury–cadmium–telluride (HgCdTe), platinum–silicide (PtSi), or indium–antimonide (InSb) material technologies. The array is then attached to an integrated circuit, which functions as an analog multiplexer, translating the signal coming from the detectors into an image that can be displayed. This whole device is referred to as an IRFPA.

The FPA is the "eye" of any IR imaging system. A basic diagram of an FPA is shown in Figure 1-1. FPAs fall into one of two categories: scanning or staring. A scanning array uses a moving, external mirror to scan the viewing scene, while synchronized electronics read out the result line–by–line. A staring array is two–dimensional and works more similarly

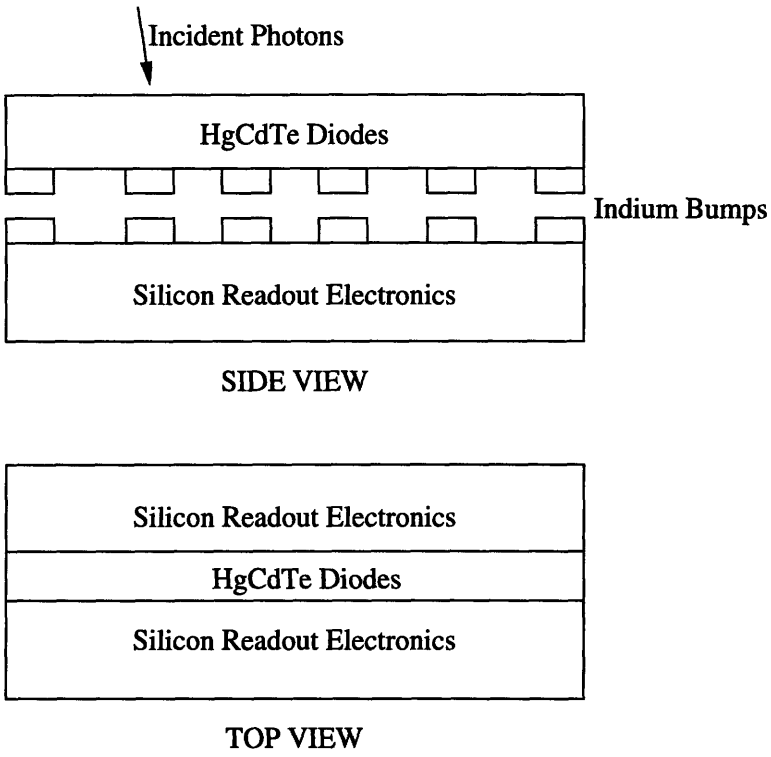

Figure 1-1: Simple diagram of an IRFPA, showing top and side views.

to a camera, taking whole two–dimensional snapshots of the viewing scene.

Both staring and scanning arrays use the same basic architecture: an array of detectors connected to an ROIC. A staring array has the advantage of not needing to "scan" a scene by using an external, moving mirror. A scanning array, however, allows more room for the ROIC layout, since the detector array constrains the designer only in one direction. Available real estate for input cells can be a significant constraint on IC designs and performance.

The best–performing, long–wave IR detectors are made of HgCdTe diodes. Other materials, such as InSb or PtSi, are not as sensitive or do not work at all at long IR wavelengths. HgCdTe detectors can be designed to work in different regions of the IR spectrum by changing the chemical composition, i.e. altering the Hg to Cd ratio. This makes HgCdTe the best choice for high–performance applications, such as strategic and tactical. The FPA in this thesis uses HgCdTe detectors attached to the silicon ROIC by indium bumps (see Figure 1-1). The indium provides a good electrical connection between the detector and the ROIC, while also providing a strong mechanical weld.

When radiation is incident upon the detector, the diode produces a photocurrent that

flows into the ROIC. The ROIC integrates the current and sends the resulting charge down its signal chain. In the end, the current is converted to a voltage that can be displayed for a user, either machine or human.

Due to the narrow band gap of HgCdTe diodes, HgCdTe arrays must be operated at cryogenic temperatures. This reduces thermally generated carriers, which would otherwise make the material intrinsic. Additionally, HgCdTe diodes have high dark current at higher temperatures, dominating any photocurrent due to incident radiation; this renders them almost useless for detecting radiation when at room temperature. Lowering the operating temperature lowers noise enough that distinctions between small changes in scene temperature can be made. To accomplish this, the FPAs are packaged in cryogenic dewars and cooled with circulating liquid nitrogen to keep the detectors at or near 77 K to detect long–wave IR radiation.

Depending upon the application, IRFPAs are designed to be either scanning or staring systems. Furthermore, the number of pixels will vary, the timing of the electronics may be altered, and critical aspects of the desired performance will change. Each new system and set of specifications requires a custom IC to be designed and built to operate optimally for the systems' specific needs. These facts make generalizations about IRFPAs difficult to make. Nonetheless, since each IRFPA shares two common components, detectors and an ROIC, determination of which piece is dominating certain performance parameters is useful. Also, since many IRFPAs use similar ROIC architectures and/or detectors, determinations of how each piece contributes to performance can be applied to many different IRFPAs.

1.1.2 Standard Advanced Dewar Assembly Infrared Focal Plane Array

The IRFPA examined in this thesis was designed for the Standard Advanced Dewar Array II (SADA–II) program. SADA is a 480–channel, scanning array. An initial "two–clip" design was manufactured several years ago, using two scanning rows of 240 channels each. The latest design is a "one–clip," with a single row of 480 channels.

This FPA was chosen for the work in this thesis for several reasons. The functionality of the multiplexer, or mux, design had already been verified on the two–clip program, and little change was made to this basic design to implement the one–clip program. This meant less design verification was needed and more time could be focused on meeting particular specifications. Another is that uniformity, the characteristic examined herein, had been

identified as a difficult specification for this design to meet in the two–clip phase, which made the one–clip a good candidate for examining influences on nonuniformities.

The SADA IRFPA was designed to function in approximately the 7 to 11 micron wavelength range, with scene–temperatures ranging from 210 to 340 Kelvin. The 480 channels each have six detectors configured in a time–delay–and–integration (TDI) scheme. TDI is a design style that sums (integrates) the current from several detectors for each channel by having each view the scene in succession (time-delay); the mechanism is similar to that of a scanning array. Its architecture reads even channels out one side and odd channels out the other. This design thus has two mirror–image signal chains of 240 channels each. Chapter 5 describes this in detail.

The ROIC is designed to run at three different master clock rates and four different gain states. Different gains allow for both high– and low–temperature scenes to be observed with greater resolution. The nominal settings were used in this work, corresponding to a clock rate of $22.8\mu s$ and gain mode 3, which corresponds to utilizing 1/3 the charge injected from the detectors to generate an output voltage.

1.2 Post–Correction Uniformity

1.2.1 Definition

Post–correction uniformity (PCU) is one of the parameters used to characterize infrared focal plane arrays (IRFPA). Since an array is made up of many channels and each channel may have a slightly different response to incoming flux, a correction scheme is needed to make the response of every channel uniform.

Raw nonuniformities of response are expected in an IRFPA. Since no detector is precisely identical in atomic make–up to another, it is reasonable that some variations in response will occur. Nonetheless, to display a useful image, some level of uniformity at the final output of the IRFPA must be achieved so that pixels viewing a uniform–temperature display a uniform picture. Even small amounts of uncorrected or uncorrectable nonuniformities can mask small variations in scene–temperature, causing the equivalent of spatial noise across the array. Several theories have been developed to address this issue of "correcting" an array with nonuniformities to achieve a uniform response (see below). The level to which uniformity is achieved is referred to as "PCU."

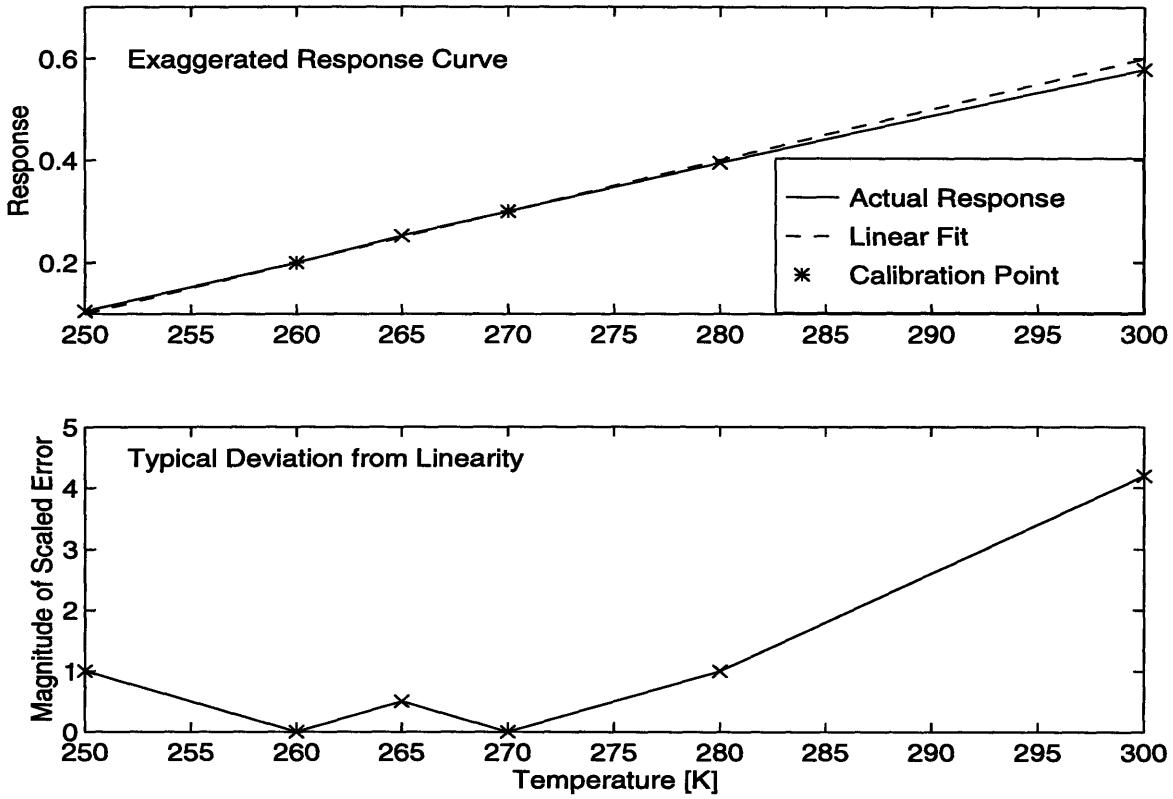

Figure 1-2: Example of a two–point correction. The top graph shows an exaggerated response, with two calibration points at 260 K and 270 K. A linear fit is made to the calibration points. The bottom graph show the absolute value of the "error" between the line and the actual response.

1.2.2 Correction Technique

The accuracy of the correction can depend not only upon the characteristics of the IRFPA but also upon the correction algorithm used to normalize response of channels. Although other techniques have been suggested [4, 10, 15], most strategic and/or tactical applications use a so–called "two–point correction" shown in Figure 1-2.

The two–point correction is a linear approximation. It is accomplished by measuring the response of every channel at two temperatures. The offset and gain of each channel can then be calculated by approximating the response as a line through those two calibration points. This correction technique has the advantage of needing only two calibration points and short calculation times, as well as being easy to implement with a scanning system—hot and cold temperature references can be viewed by the FPA at the ends of the mirror scan; it also requires a large amount of pre–correction linearity and/or uniformity in the array to work well.

Theoretically, if all channels were precisely linear but nonuniform, this correction scheme would be perfect, since all linear "errors" are corrected. Similarly, if all the channels were nonlinear, but shared a common "shape," i.e., if only offset caused nonuniformities, a linear correction scheme would result in perfectly uniform responses.

A linear correction is predicted to work well, since detectors theoretically respond linearly to incident flux:

$$V(T) = \frac{q\eta\Phi(T)t_i}{C}, \tag{1.1}$$

where V is the detector signal voltage; q is the charge on an electron in coulombs; η is the detector quantum efficiency, usually $\simeq 70\% - 90\%$; $\Phi(T)$ is the photon flux in photons/second; t_i is the integration time in seconds; and C is the equivalent integration capacitance in Farads. Thus, if the ROIC is designed with good linearity in its active range, the offset and gain variations from detector–to–detector or channel–to–channel would be corrected. Similarly, if the ROIC were identical across all channels, while nonlinear, it would still be fully correctable.

Unfortunately, nonuniformities still appear after correction. This indicates that the ROIC response is not linear and/or uniform or that the predicted linear response of the detectors is incorrect or some combination of these two.

1.2.3 Calibration Temperatures

After deciding on a correction technique, such as the two–point correction used in this work, picking the calibration temperatures is important and can greatly influence the results. Many researchers [6, 7, 10, 11, 17], have shown that the smallest post–correction nonuniformity (PCNU) is observed when the calibration points are as far apart as possible.

This makes good sense. As with any nonlinear function, a linear fit will be better if it uses the whole range of values, and not just a small subset in the middle. Also, choosing temperatures that are farther apart allows the linear approximation to interpolate, rather than extrapolate responses to other temperatures.

Since response across the array is set to be exactly uniform at calibration temperatures, they will naturally be the scene–temperatures at which the FPA performs best. This can be another important factor in choosing calibration temperatures. Unfortunately, when an FPA is designed to work over a wide range of temperatures, the most–often viewed

temperatures, and thus the ones at which the FPA should perform best, often fall in the middle of the range. This results in calibration temperatures for some applications being narrowly–spaced in the middle of an operating range. In these cases, as is the case in this thesis, pre–correction uniformity of response becomes even more important to achieve acceptabel levels of PCU.

1.2.4 Statement of Problem

Unfortunately, following correction, many IRFPAs continue to exhibit nonuniformities between channels. These discrepancies result in a "fixed–pattern" of noise, also known as spatial noise, in every frame of data. Although many people have examined this difficulty, the causes of PCNU remain poorly understood and have not been well–characterized. The subject of this work was to better characterize PCNU.

The approach taken to determine the influences on PCNU in this thesis was to first divide the possible causes into three categories: testing, ROIC, and detector parameters. The coupling between detector nonuniformities and ROIC nonlinearities can be treated as a fourth category, but strongly depends upon their separate contributions. Several factors influencing PCNU for each of these categories were considered to be potentially significant; these are indicated in Table 1.1 and are described in more detail in following chapters. The idea is to isolate each of these elements and then pinpoint which of their particular facets influence the final results. Testing was addressed first, since, if the test results could not be trusted, other analysis on the data would be useless. Following the verification of the test equipment, attention could be focused on the ROIC and detectors.

Table 1.1: Possible influences on post–correction nonuniformities.

Test	**Detector**	**ROIC**
electronic drift	$1/f$ noise	temporal noise
blackbody stability	spectral response	layout architecture
FPA temperature stability	physical variations	processing variations
	coupling between detector nonuniformities and ROIC nonlinearities	

1.3 Outline

Chapter 1 of this thesis provides an introduction to the problems with PCU, as well as describing the SADA II 1–clip parts. Chapter 2 reviews prior work on the problem, as well as examining in detail the possible detector–related contributions to nonunifomities. Chapter 3 contains a description of the test equipment and procedures. Chapter 4 presents the results of testing several FPAs. It also discusses the contribution to PCNU from the test equipment, including how the errors from testing procedures were remedied. Chapter 5 provides an analysis of the results in Chapter 4, with close attention paid to the ROIC. Chapter 6 details the conclusions reached in this work, as well as some recommendations for further examination of the problem.

Chapter 2

Possible Influences and Previous Work

Many different researchers have addressed the problem of nonuniformity. Most concentrated on a single facet of the problem, e.g. detector–contribution or test equipment difficulties, and, with a few exceptions [6, 14, 18], used predicted results rather than real data in their analyses. Their relevant work is discussed in the following sections.

2.1 Two–Point Correction

Perry and Dereniak [14] analyzed the two–point correction on an IRFPA. They showed that it completely removes additive and multiplicative (the offset and gain) nonuniformities from the response curve. Their modeled predictions showed that the PCNU would be below the other temporal noise in the system (e.g. from electronic drift); however, they had difficulties when testing an actual PtSi FPA and were unable to explain conclusively the experimentally–determined larger errors by measuring detector nonlinearities. Their hypothesis was that the multiplexer on their sensor was the cause; this was supported by variations in performance between the odd and even channels. Work for this thesis supports the hypothesis that the multiplexer contributes to residual nonuniformities.

2.2 Test Equipment

Test equipment and set–ups for analyzing PCU can vary widely from laboratory to laboratory; however, all share a common goal: evaluating the performance of an FPA. A few researchers have shown how elements of a test configuration can contribute to PCNU. O'Neill [13] showed that drift within test equipment can contribute to poor uniformity results. He states that knowing the stability of the data acquisition system (DAS) and other electronics is necessary so that test results can be trusted. If the electronics are drifting, the results from the FPA will drift too, causing "false" errors. As the electronics drift, the voltage off the FPA will appear to be drifting too. Since this is a nonuniform effect across the array, it is not linearly correctable.

The accuracy with which values are measured and the amount of noise in the equipment are also important contributors to PCNU [10, 13]. If the resolution of the DAS is too coarse, small variations in response may appear larger than they actually are and result in large PCNU. As an exaggerated example, if the DAS can only distinguish 0.5 V increments, the difference between a 1.45 V response and a 1.43 V response would appear as a 0.5 V difference, rather than the actual 0.02 V difference. Similarly, if a lot of noise is present in the system, it can cause "spikes" at certain times that are not indicative of the FPA response, but will appear as uncorrectable nonuniformities when analyzed.

The stability of the blackbody source also is important; if uniform results are expected, the scene–temperature must remain uniform during testing. Some work has been done measuring the stability and uniformity of flux across the surface of wide–area blackbodies that are often used for PCU testing. A close monitoring of the temperature of a blackbody has been determined to be necessary during testing [2]. A blackbody drift in temperature would have a similar impact to the drift in the electronics described above—drift in response to incoming flux will appear falsely as nonuniform FPA channel responses.

2.3 Detectors

The most work on PCNU has focused on detectors. Part of the reason for this is that many believe the detectors are the source of the problem. Some claim that uniformity is limited by variation in the physical properties of a detector array, such as size of the detectors or detector impedance, which affect how the detector responds to incoming flux [7, 12].

This may be a fundamental limit in response uniformity, since, if all other factors were eliminated, variations in detectors from the fabrication process would still exist and limit performance. Other characteristics of detectors, as well as their physical variations, can influence the IRFPA more than the fabrication of the detectors [7]. $1/f$ noise and spectral shape variations are two that have been shown to affect the correctability of IRFPAs [9, 11, 15, 17, 18]. These are discussed more in the following sections.

2.3.1 Physical Characteristics

A detector array is not perfectly uniform. Variations from the growth of the material or variations in dopant concentration occur frequently. These variations change how a detector responds to incoming photons by altering its dark current, quantum efficiency, or dynamic resistance. The largest physical variations in an array usually occur in detectors that are physically far apart from one another; detectors close to one another are likely to be subject to more similar aberrations in the fabrication process than those spaced farther apart.

Karins analyzed in detail the contribution of detector variations to PCNU [7]. He focused on the detectors' response to incoming flux at given wavelengths, which is calculated by:

$$R(\lambda) = \Phi \int_0^\infty \alpha(\lambda) e^{\alpha(\lambda) z} dz \int_{-a/2}^{a/2} \int_{-b/2}^{b/2} e^{\frac{-r(x,y,z)}{l_m}} dx dy \tag{2.1}$$

where $R(\lambda)$ is the response to a wavelength, λ, Φ is incoming flux, α is the absorption coefficient, z is the depth, a and b are the pixel lateral dimensions, l_m is the diffusion length of minority carriers, and $r(x, y, z)$ is the minimum distance to the depletion region. (Compare this to Equation 1.1.) Equation 2.1 shows the wavelength–dependence of responsivity and the impact of local detector geometry. Due to process variations, the dependence can vary from detector to detector. The response of the detector $R(\lambda)$ directly relates to PCU. Variations detector characteristics affect the integral of Equation 2.1, which alters the linear relationship between Φ and detector current. Since PCU is impacted by nonlinearities, particularly if they vary from detector–to–detector, as z, a, b, l_m, and α may, $R(\lambda)$ affects PCU.

Karins then calculated how various parameters of detector design influenced PCNU. He concluded that the physical parameters of a detector at most contribute a 0.5% error to linearity [7]. Since SADA allows for a 5% error in linearity, the majority of the nonlinearity

in the FPAs must be from other factors. Data examined in this work supports this theory, discussed in Chapter 5.

2.3.2 $1/f$ Noise

$1/f$ noise describes a current fluctuation having a spectral density that is proportional to $1/f$. It appears in infrared detectors at low frequencies as a line with slope $1/f$. This noise causes fluctuations in detector current that increase logarithmically with observation time [17]. If these fluctuations are significantly large over the calibration period, they can influence PCU. Since each pixel generates its own $1/f$ noise uncorrelated to every other pixel, it clearly can contribute to spatial nonuniformity of an IRFPA.

Scribner *et al.* [17] examined this phenomenon. They accurately predicted the variance of response for measurements made within 30 seconds of one another but found inexplicable errors if calibrations were made at longer intervals. They also estimated that the statistical distribution of $1/f$ noise across an entire IRFPA would be the same as one pixel's drift. Scribner *et al.* [18] reexamined the problem and proved that the assumption of an identical but uncorrelated distribution of $1/f$ noise across the array was valid. They also confirmed the poor relation between predicted variations in correctability over time due to $1/f$ noise and the actual measured values. They theorize that this is due to contribution of $1/|f|^n$ not $1/f$ noise, though this is not proven [18].

2.3.3 Spectral Shape

Spectral response describes how a detector responds to different wavelengths of light. An ideal photodiode exhibits a linear relationship between incident photons and generated electrons, or current, that is independent of wavelength up to the cutoff of the material. Thus, the spectral response of an ideal detector is flat for $\lambda < \lambda_c$ and zero for $\lambda > \lambda_c$, as shown in Figure 2-1. Real spectral responses tend to be "soft" or rounded near the cutoff wavelength of the detector as also shown in Figure 2-1 (the cut–on wavelength is determined by the cold filter). This can be influenced by many characteristics of the detector, including doping characteristics, etching profiles, etc. In an attempt to minimize the impact of varying spectral shapes, a cold filter is placed between the scene and the detectors, which forces a uniform bandpass for each detector.

The actual cutoff of the detectors is chosen to be very close to the cutoff wavelength

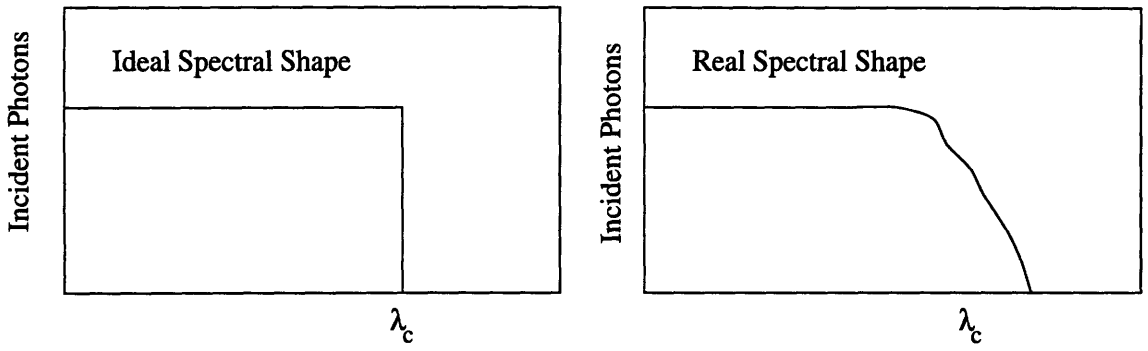

Figure 2-1: Spectral shapes of an ideal vs. real photodiode.

of the cold filter, because the shorter the cutoff wavelength of a detector is, the higher its impedance is and, thus, its leakage current is smaller. A detector cutoff wavelength that is close to that of the cold filter also maximizes the available dynamic range by not designing the detector to operate at unused wavelengths. Due to the softness of the spectral cutoff of real detectors, however, in order to limit all SADA detector cutoff variations within 0.25μm of the desired cutoff wavelength, the filter would have to cutoff at least 0.4 microns shorter than the average diode cutoff [9]. This causes an unacceptable loss in performance.

Mooney *et al.* [11] determined that spectral nonuniformities could not be corrected, because the error induced by them is nonlinear. This is due to the dependence of detector spectral shape on relative flux and temperature. The cutoff wavelength of a detector can affect PCNU by causing nonuniform responses at longer wavelengths. Thus, if detectors in channel 194 have much "softer" spectral shapes than detectors in channel 193, channel 194 will respond less to incoming flux at lower temperatures than channel 193.

A cutoff wavelength of a detector, λ_c, can be calculated from

$$\lambda_c = 1.24/E_g \tag{2.2}$$

where E_g is the band gap in eV. The cold filter changes the equation for detector response to incoming flux, Equation 1.1, by limiting the incoming flux, $\Phi(T)$ in the following way [5]:

$$\Phi(T) = \int_{\lambda_l}^{\lambda_c} \frac{2c}{\lambda^4(e^{hc/\lambda kT} - 1)} d\lambda \tag{2.3}$$

where λ_l and λ_c are the wavelength limits of the cold filter and c is the speed of light, h is Planck's constant, and k is Boltzmann's constant.

Thus, using Equation 1.1 and 2.3, one can acquire the total detector response, $V(T)$:

$$V(T) \simeq \int_{\lambda_l}^{\lambda_c} \frac{2cq\eta(\lambda)t_i}{C\lambda^4(e^{hc/\lambda kT}-1)}d\lambda. \tag{2.4}$$

Note that η, quantum efficiency, is also a function of wavelength.

On the other hand, Maschhoff [9] has argued that an accurate model of the influence a spectral response has on detector output could predict the error and correct for it. Maschhoff investigated the contribution of spectral variation to PCNU, but was unable to corroborate his model with any experimental results [9].

2.4 Read–Out Integrated Circuit (ROIC)

Little research has been done on the ROIC itself. Some of this is due to its being so application–specific; some is due to the assumption that the detectors are contributing more to the error. Small nonlinearities in the ROIC signal chain are not unusual, but uniformity across an array is usually good. Herzog and Williams [6] discuss how nonlinear characteristics, particularly in capacitance, of the signal chain of an ROIC can affect PCNU. This thesis examines contributions from the ROIC in great detail in Chapter 5.

2.5 Coupling between the ROIC and Detectors

Viewing the entire IRFPA, instead of the individual pieces, the interface between the detector and the ROIC is a possible contributor to PCNU. There are a couple of ways this can happen. The first is that the ROIC contains some uniform nonlinearity, and the detector array has some nonuniformity but responds linearly to flux as predicted in Equation 2.3. Either of these alone would be correctable with the two–point correction; however, coupled together, they result in nonlinear nonuniformities, which are not correctable.

A good example of this effect is variations in quantum efficiency in the detectors. Figures 2-2 and 2-3 display how the phenomenon occurs. Figure 2-2 displays a possible ROIC response curve and its deviations from linearity. Figure 2-3 shows how varying only detector quantum efficiency (QE) shifts the current coming in along the ROIC curve. The combination of the two effects results in the "W-curve" shown in Figure 1-2 "shifting" up and down, which directly impacts PCNU.

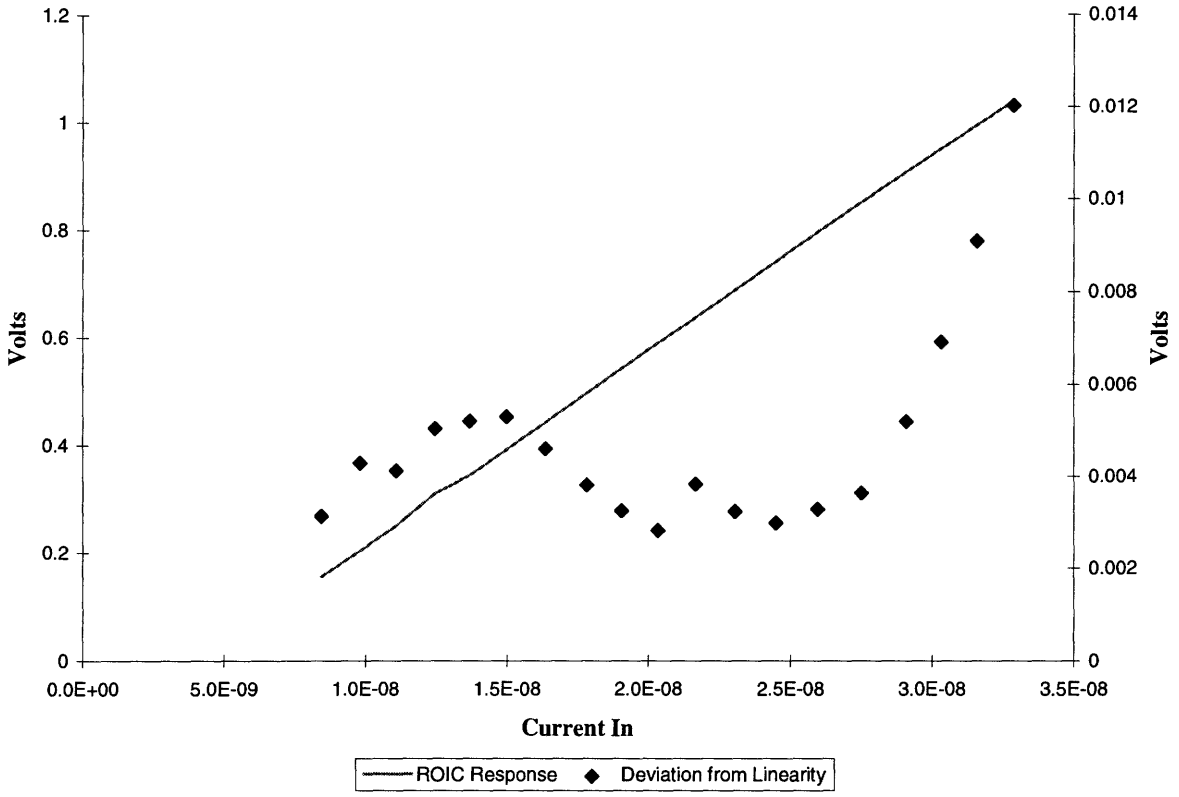

Figure 2-2: Possible ROIC response curve and deviation from linearity [Volts vs. Current In].

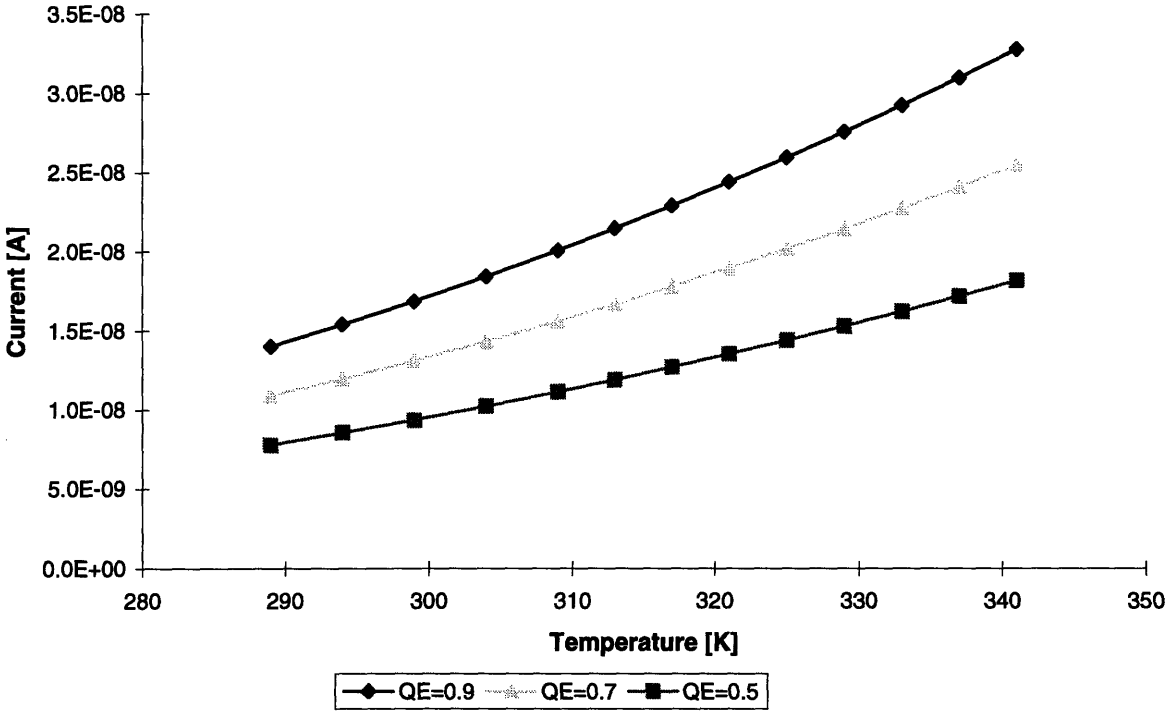

Figure 2-3: Effect of varying quantum efficiency (QE) on detector response to scene–temperatures.

Chapter 3

Testing

3.1 Test Station

Evaluation of both the ROICs and the FPAs is performed on the test station, shown in Figure 3-1. It includes a Hewlett Packard (HP) workstation that controls the test and drives all the instruments, a printer, a personal computer (PC) for data reduction, Pulse Instruments clock and bias generators, a function generator that sets the clock rate for the device under test (DUT), an oscilloscope, a wide–area blackbody and controller, a cryogenic test–dewar that contains the DUT, and a 16–bit data acquisition system (DAS). The software controlling the tests is written in HP BASIC. This test station is a standard set–up for analyzing IRFPAs. For ROIC testing, the blackbody is not used.

The cryogenic dewar is a pour–fill dewar, which is kept under vacuum and filled with liquid nitrogen that is periodically "topped–off" during testing. The nitrogen keeps the DUT at 77 Kelvin. The vacuum is necessary to keep moisture in the atmosphere of the dewar from frosting over the part, thus rendering it inoperable. The temperature inside the dewar can be monitored externally. The dewar is connected to the test electronics through BNC cables and either a "test box" or an electronic board. The "test box" is used to optimize FPA operating points, such as detector bias voltage, for minimum noise, maximum dynamic range, etc., while the board is hard–wired and is used to control the FPA when it is fully operational. Optimization for uniformity is not performed. In testing for this thesis, previously–optimized operating points were used.

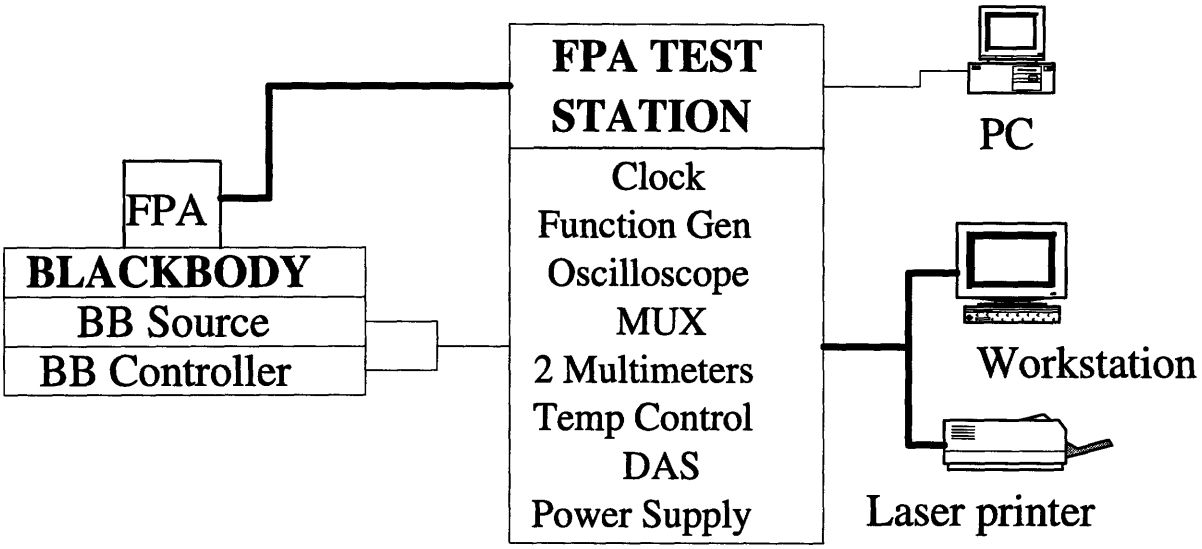

Figure 3-1: Schematic of FPA test station.

3.2 Test Software

As mentioned above, the software controlling all the test equipment is written in HP BASIC. Most tests are fully automated and the software can run a whole battery of diagnostic tests on an FPA at once, including descriminating out "bad" detectors, calculating D*, etc. Although the SADA testing software is long and detailed, it contains only two basic ways of acquiring data.

The first is called a "Pixel Test." This test addresses a single channel of the FPA and records a specified number of measurements off of it. For example, one can address channel 156 and specify 1024 readings[1] to be made. The software then averages 1024 readings off of channel 156 and returns the average value, the standard deviation of the readings, and the minimum and maximum values. Since it takes a reading once every master clock cycle, 1024 readings take on the order of $20ms$.

The second data acquisition mode is called a "Channel Test." The Channel Test takes data more in the manner which the FPA will ultimately operate. It sweeps across the array, taking a specified number of readings at each channel. This is referred to as a "frame of

[1] A large number of readings lowers random noise by a factor of $1/\sqrt{\#ofreadings}$.

data." It then returns these averaged outputs. The user specifies the number of averages to be taken, such as the 1024 specified above, and then the software does the rest, stepping across the array, sequentially taking 1024 readings at each channel. The total time needed for this is simply $1024 \times 480 \times 22.8\mu s = 11.2s$.

3.3 ROIC Linearity Testing

The ROIC was tested for linearity, since linearity and PCU are related, particularly when using a linear correction scheme [14]. The SADA ROIC was designed with two test–input setups, a single–input and a global–input. Both of these tests provide the same information and are good checks of one another.

3.3.1 Single–Input Test

The single–input linearity circuitry consists of a switch that, when closed, allows current from an external source to flow into the input where a detector would normally be attached. By turning this switch on and attaching a $100M\Omega$ resistor, one can input selected amounts of current by applying a known voltage across the resistor. A large, high–precision resistor is used to simulate accurately the small currents ($1nA - 1\mu A$) that a detector would produce. The other end of the resistor is tied to V_{bias}, which is used to set the bias voltage across the detector when the ROIC is operating in an FPA. This is set to $7.68V$. The other node of the resistor is then varied over a range of voltages to produce a variety of currents.

In order to determine the linearity of the ROIC, initially it is configured to sum all six–in–TDI detector inputs at once. If a nonlinearity is observed in a particular channel, one can then set the ROIC to view each TDI input individually. This helps determine whether the nonlinearity is due to a single input cell or something inherent in the entire channel. Because only a single channel can be examined at a time, this is called a single–input test.

Unfortunately, when this test was run on the SADA–II ROICs, unanticipated results emerged. It appeared as though the first detector input in a channel responded as expected, but then each successive detector input did not start responding until some critical voltage was obtained. (See Figure 3-2 for an example of this.) This caused large nonlinearities to appear in the overall output as seen in Figure 3-3.

Since overall FPA testing had not displayed this kind of nonlinearity, it was assumed

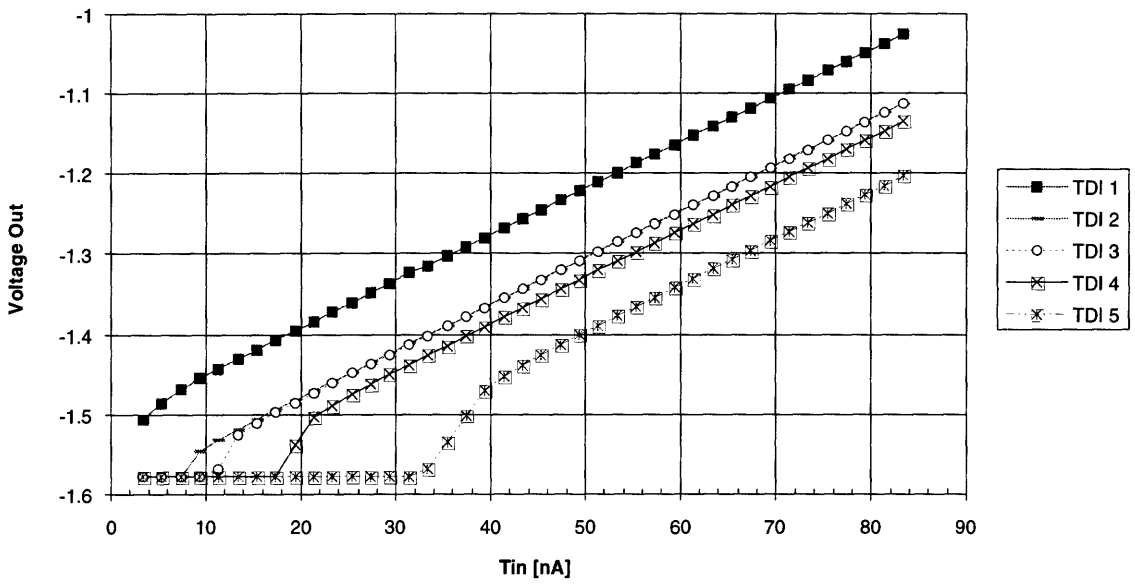

Figure 3-2: Linearity plot for individual detectors–in–TDI using single–input test.

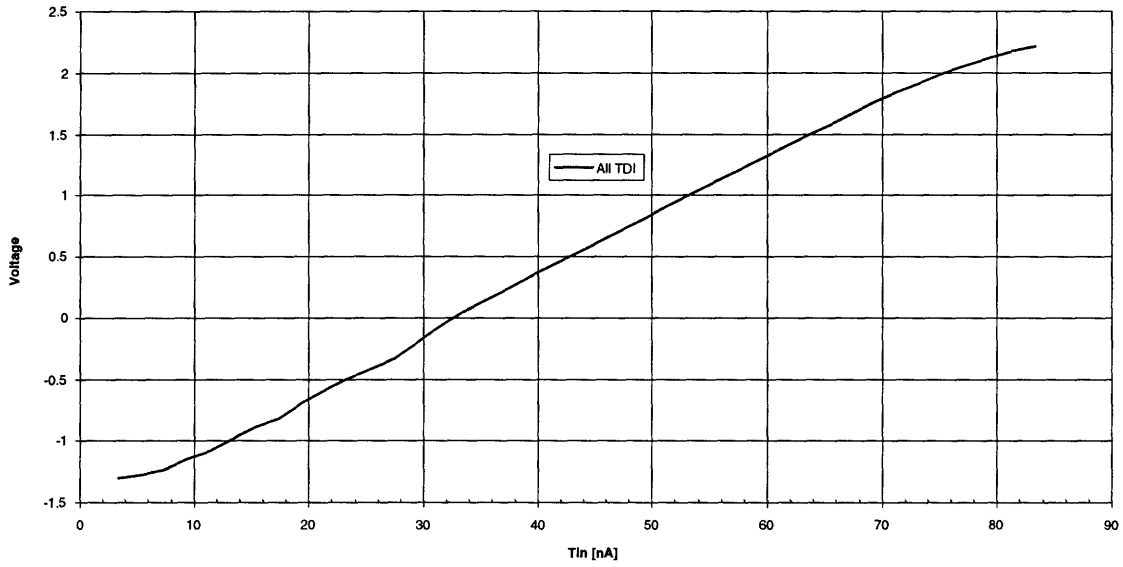

Figure 3-3: Linearity plot for all six–in–TDI using single–input test.

that some aspect of the test was causing the unexpected result. This was attributed to the capacitive switching necessary to select individual detector inputs[2]. Although this was not a conclusive answer, the subject of this work was not to perfect a single–input linearity test, but to use accurate linearity measurements for further analysis. Fortunately, the SADA II 1–clip part was designed to allow for a global–input test for linearity. This test was then implemented.

3.3.2 Global–Input Test

The second test input is a global input shown in Figure 3-4. The global input consists of two switches and a capacitor. A voltage ramp is applied to the capacitor, and then the first transistor switch is closed and the current flows into the signal chain. This charge flows into all the channels at once, (see Figure 5-1 for a diagram of the signal chain) thus greatly reducing the number of capacitive switches needed. After the charge is switched into the signal chain, the capacitor voltage is reset to V_{bias} by the other transistor switch. The detailed timing of these three signals is displayed in Figure 3-5.

The signal is then measured by using the Channel Test to record the voltages. By selecting several different heights for the voltage ramp, a linearity plot could be generated for every channel. The global input allows much more information about an ROIC to be determined quickly than the single–input test. To obtain linearity characteristics of all channels, the single–input test must be run 480 times. The global input need only be run a number of times equal to the number of points on the linearity curve, since it takes data on all channels at once. Since the labor–intensive part of the test becomes generating a complete linearity curve, a more practical result of this test is the ability to determine the capacitance of a channel. The capacitance of several ROICs was calculated. The results and analysis of this test are discussed in Chapters 4 and 5.

3.4 FPA Testing

Testing the FPAs involved two different tests: recording the actual channel output of the FPA to various scene temperatures, and monitoring the temperature of the FPA.

[2]This hypothesis was set forward by Daniel Lacroix and Frank Jaworski, senior ROIC designers at Lockheed Martin IR Imaging Systems, Lexington, MA.

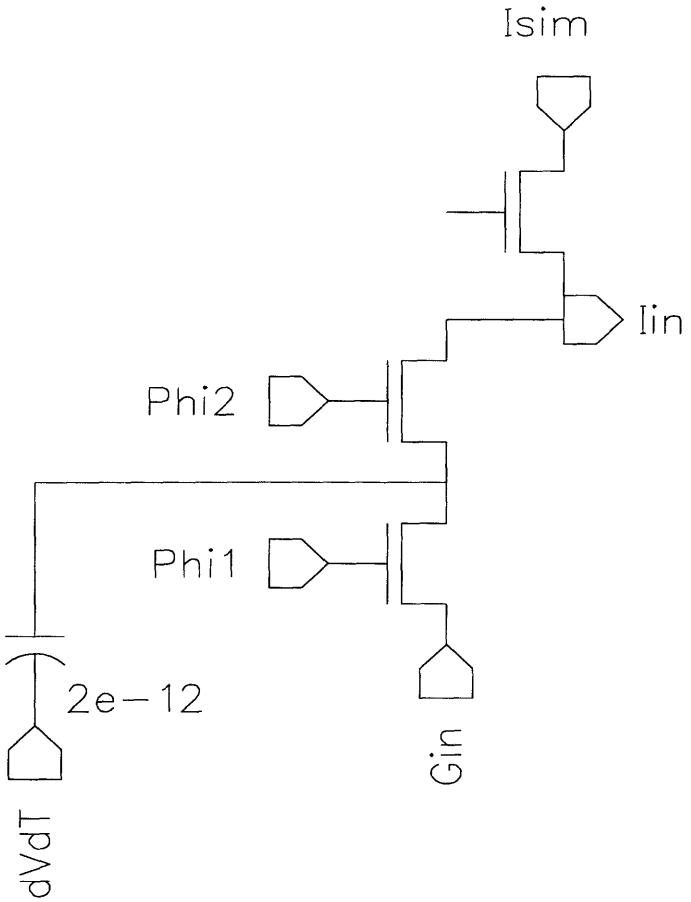

Figure 3-4: Diagram of ROIC global–input test circuitry.

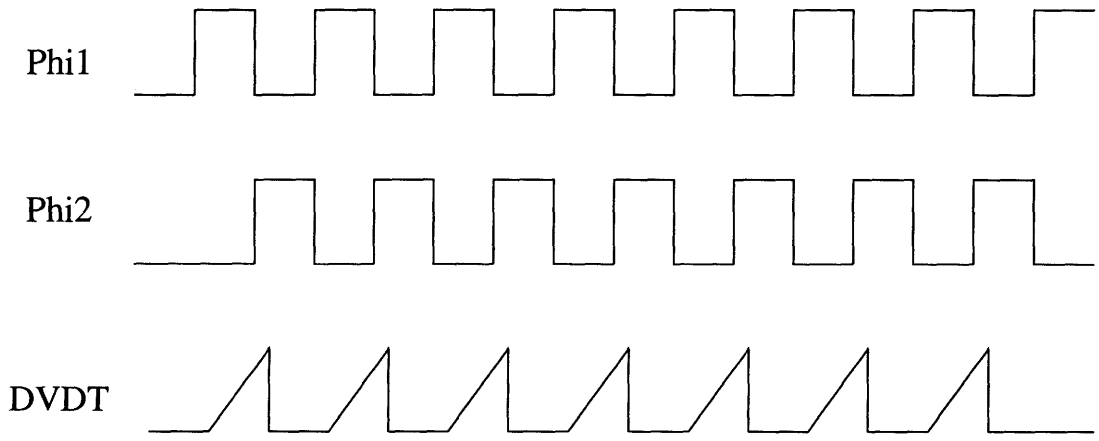

Figure 3-5: Detailed timing of global–input test control signals.

3.4.1 Output Tests

An uncorrected linearity plot was created by taking frames of data at the six SADA–specified PCU temperatures: 290, 300, 305, 310, 320, and 340 K. A plot of volts vs. $\Phi(T)$, the flux at each temperature, which ideally would be a straight line, could then be drawn for all 480 channels of the FPA–under–test. Both linearity and PCU, as defined by the SADA Development Specification [20] described in Section 3.5, can then be determined by performing specified calculations on the results of the test.

3.4.2 Temperature Stability Test

The temperature of the FPA is assumed to be constant during testing. This is due to the fact that it is constantly cooled with liquid nitrogen, which is at 77 K. If this assumption is proven false, significant impact on PCU results will occur [14]. This is discussed in much more detail in Chapter 4.

Two mechanisms exist for monitoring the temperature of an FPA–under–test. The first is an external temperature sensor that can be attached to the dewar. This accurately records the temperature inside the dewar. The temperature of interest, though, is not the temperature of the dewar, but the temperature of the FPA itself. Thus, the second method is more appropriate here.

The second method of monitoring the temperature of the focal plane is to place a calibrated diode on the package in which the FPA is mounted. This diode has a known response to temperatures of 4 K and 77 K, acquired by immersing it in liquid helium and nitrogen, respectively. Its response at other temperatures can then be predicted. Thus, by recording the voltage off this diode during testing, the temperature of the focal plane can be monitored closely and accurately.

Only the second method was used in testing for the work presented here. The temperatures of several FPAs were monitored over long periods of time, from 0.5 to 5.0 hours. This was done to determine the time constant for fully cooling down a test–dewar, as well as discovering how stable the temperature of the FPA was over the duration of a PCU test. Again, results of this testing will be presented and discussed in Chapter 4.

3.5 SADA Specification

The specification for the SADA program defines linearity, PCU, and other related characteristics of a focal plane. The following describes how PCU will be determined and defined for the rest of this work, as well as how the terms "linearity" and "responsivity" will be applied. The SADA specification requires all linearity and PCU tests to be performed with the device at 77 ± 1 K and not to deviate more than 0.5 K from that set temperature during testing [20].

Each of the following calculations was automated using Visual Basic software. By transferring data from the Channel Test described above from the HP on the test station to a personal computer, these calculations could be performed quickly and automatically. Also, the HP Basic environment is not conducive to in–depth data analysis; it is designed for large amounts of repetitive testing, not manipulations of produced data.

3.5.1 Post–Correction Uniformity Definition

PCU is defined based on comparisons between channels. First the voltage at every temperature, T_x, for each channel,i, is reported. Then, these channel voltages, $V(i, T_x)$, have the response at calibration temperature T_2, $V(i, T_2) \equiv O_i$, subtracted from each of them, creating:

$$V_o(i, T_x) = V(i, T_x) - O_i \tag{3.1}$$

for $x = 1, ..., 6$ and $i = 1, ..., 480$. O_i is defined as the offset for channel i.

The gain, G_i, is then calculated by:

$$G_i = \frac{\sum_{j=1}^{480} V_o(j, T_4)}{480 \times V_o(i, T_4)} \tag{3.2}$$

or the average voltage at T_4 divided by ith channel's voltage at T_4. Now, a new, fully–corrected voltage for each channel can be calculated from V_o and G_i:

$$V_c(i, T_x) = V_o(i, T_x) \times G_i. \tag{3.3}$$

Thus, effectively, all additive and multiplicative nonuniformities have been removed from the responses across the array, by approximating each channels' response as a straight line

passing through an arbitrary $V(T_2) = 0$ and the average value of $V(T_4)$ [20].

Each V_c is then compared to the average V_c of its sixty nearest neighboring channels through the following calculation:

$$V_{ce}(i, T_x) = V_c(i, T_x) - \frac{\sum_{k=i-30}^{i+30} V_c(k, T_x)}{60}. \tag{3.4}$$

The measured deviations, $V_{ce}(i, T_x)$, are reported relative to a nominal system noise voltage, $Vn = 830\mu V$. If $V_{ce}(i, T_x)$ varies more than a certain number of Vn from the average, it fails the PCU test. Table 3.1 shows the allowable differences for each PCU temperature.

Table 3.1: SADA II 1–clip PCU specification for each blackbody temperature.

Blackbody Temperature	**Allowable "Error" in Vn**
T_1	± 1
T_2	0
T_3	± 1
T_4	0
T_5	± 2
T_6	± 4

where $Vn = 830\mu V$, and temperatures T_1 through T_6 are 290, 300, 305, 310, 320, and 340 Kelvin [20].

3.5.2 Linearity Definition

Linearity is calculated and defined for each channel as follows:

1. $dV/d\Phi$ is the change in voltage per change in computed flux between successive PCU temperatures;
2. $DV/D\Phi$ is the change in voltage per change in computed flux between the highest and lowest PCU temperatures;
3. "nonlinearity" is the difference between the maximum and minimum values of $\frac{dV/d\Phi}{DV/D\Phi}$;
4. "linearity" is (1−"nonlinearity").
5. Every channel must have linearity greater than 0.95, or less than 5% nonlinearity.

Linearity is important because, as stated in Chapter 1, if all the channels were linear, a two–point correction would make the responses uniform. Since, as seen in Chapter 4, many channels of the FPAs fail this linearity test, uniformity becomes more important

3.5.3 Responsivity and DC Offset Uniformity

Two other SADA FPA specifications relating to PCU are responsivity and DC offset uniformity. These are effectively pre–correction uniformity standards that each FPA must meet.

DC offset uniformity is also called the "fixed pattern noise" requirement. It demands that each uncorrected voltage response at the nominal background temperature, $V(i, T_1)$, be within $\pm 640mV$ of the average $V(T_1)$.

The responsivity requirement defines $R_i \equiv 1/G_i$, where G_i is defined in Equation 3.2. Each R_i must fall in a window around R_{ave}, the average of all R_i's [20]:

$$0.65R_{ave} \leq R_i \leq 1.35R_{ave} \tag{3.5}$$

Note that this uses the gain values before they are "corrected" by normalizing to the average gain.

These two requirements eliminate especially nonuniform channels from consideration before PCU calculations are even made. Since PCU calculations involve averages of nearest neighboring channels, this preliminary elimination of grossly nonuniform channels is necessary for realistic, accurate results, as shown in Chapter 4. These pre–correction specifications also insure a certain "raw" uniformity of response across the array.

Chapter 4

Results of PCU Testing

4.1 Testing Issues

4.1.1 Blackbody Temperature

The blackbody temperature stability, though it can affect PCU results considerably, was determined not to be an issue. The calibration of the wide–area blackbodies used here was performed by the manufacturer, CI Systems, who guarantees stability of its blackbodies temperature to within a few milliKelvin over hours. Each blackbody is equipped with a thermometer that allows the user to set and monitor its temperature. This indicated that the guaranteed level of stability was in fact being met. The thermometer is accurate to within ± 0.01 K.

By calculating the effect a change of a few milliKelvin might have on the detectors (see Eq. 2.3 for detectors' temperature dependence) it was found that the contribution was at least an order of magnitude smaller than what was being observed on PCU values. Table 4.1 shows how varying scene temperatures affects the photocurrent of a detector, and consequently PCU results. The table shows that at most 0.3% variation in current would occur for blackbody fluctuations of 0.1 K, ten times the sensitivity of the temperature sensor of the blackbody. Temperature fluctuations are more likely at the higher scene temperatures, since the difference from the ambient temperature is greatest then. At the higher scene temperatures, even variations of 0.5 K result in only 0.8% variation in photocurrent.

Another indication that blackbody stability does not affect PCU measurements is the time which the PCU measurement takes. After changing temperatures (e.g. T_2 to T_3), the

Table 4.1: Modeled effect of blackbody temperature variations on the photocurrent in detectors.

Temperature [K]	Deviation	Photocurrent Error $[\Delta I_o/I_o]$	Voltage Error $[Vn]$
240	±0.1	0.003	0.08
310	±0.1	0.002	0.11
310	±0.5	0.008	0.44
340	±0.5	0.007	0.63

test software waits for the blackbody temperature to be stable for at least 60 seconds before beginning to take data. Then, the actual time to make readings on all channels is less than 15 seconds:

$$t_m = 1024 \times 480 \times 22.8\mu s = 11.2s \tag{4.1}$$

for 1024 readings at every one of 480 channels. Thus, the blackbody would have to fluctuate by degrees of temperature in 11 seconds to affect the PCU measurement at the set temperature.

The third, and perhaps most convincing, indication that blackbody stability is not affecting PCU is the results themselves. A drift from the blackbody in a $10s$ period would appear as a gradient in response across the array. No such gradient appears in any measurement, except that which is attributable to focal plane temperature drift (see discussion below).

4.1.2 Focal Plane Temperature

Focal plane temperature, T_f, is an important factor in PCU determinations, because it affects a number of detector operating parameters, including R_d, the dynamic resistance, λ_c, the cutoff wavelength, and η, quantum efficiency. The factor that most significantly affects PCU due to focal plane temperature variations is the detector current:

$$I_o = I_{sat}(e^{qV_{bias}/kT_f} - 1) - I_p \tag{4.2}$$

where I_{sat} is the saturation leakage current from minority carrier diffusion; I_p is the photocurrent, which depends on the quantum effieciency, η, which is also weakly T_f–dependent; and V_{bias} is the bias voltage.

Differentiating Equation 4.2 with respect to T_f and discounting the minor affect from

I_p gives

$$\frac{dI_o}{dT_f} = -I_{sat}\frac{qV_{bias}}{kT_f^2}e^{qV_{bias}/kT_f}. \tag{4.3}$$

Similarly, differentiating with respect to V_{bias} gives

$$\frac{dI_o}{dV_{bias}} = \frac{1}{R_d} = I_{sat}\frac{q}{kT_f}e^{qV_{bias}/kT_f}. \tag{4.4}$$

These two together give the useful equation

$$\frac{dI_o/dT_f}{dI_o/dV_{bias}} = R_d\frac{dI_o}{dT_f} \tag{4.5}$$

$$\Rightarrow \frac{dI_o}{dT_f} = \frac{V_{bias}}{R_d T_f}. \tag{4.6}$$

Since V_{bias} is held nominally at $-20mV$ during testing, this implies a $1Vn$ change in output for every $67mK - 330mK$ change in T_f. The range stems from variations in R_d, typically $4M\Omega - 160M\Omega$, across the detector array.

T_f is nominally held at 77 K during testing. The absolute value of this temperature is much less important than its stability over time for PCU considerations. As described in Chapter 3, a calibrated diode is used to monitor both the absolute and relative temperature fluctuations during testing.

A good illustration of how focal plane temperature drift drastically affects PCU is shown in Figures 4-1 and 4-2. They display how stabilizing focal plane temperature directly affects PCU. Figure 4-1 is PCU measurements on T_1, 290 K on a test started at time=0. Figure 4-2 is the same focal plane, same PCU temperature, same cool–down, only the test was run starting a time=90 minutes. The difference is significant. The drift that so clearly appears in the first plot is nearly absent from the second.

A typical dewar has a cool–down time constant, τ, of 200 seconds.[1] This calculation was based on the thermal conductance and mass of the FPA cold filter. This leads to a 40 minute waiting time for fluctuations to fall below 10 mK, assuming a 300 K starting temperature. This matches the experimental data well. Figure 4-3 is a plot of FPA temperature versus time. It can clearly be seen that the temperature does not stabilize until more than 30

[1]Dr. Paul Murphy, test dewar designer at Lockheed Martin IR Imaging Systems, Lexington, MA, personal communication.

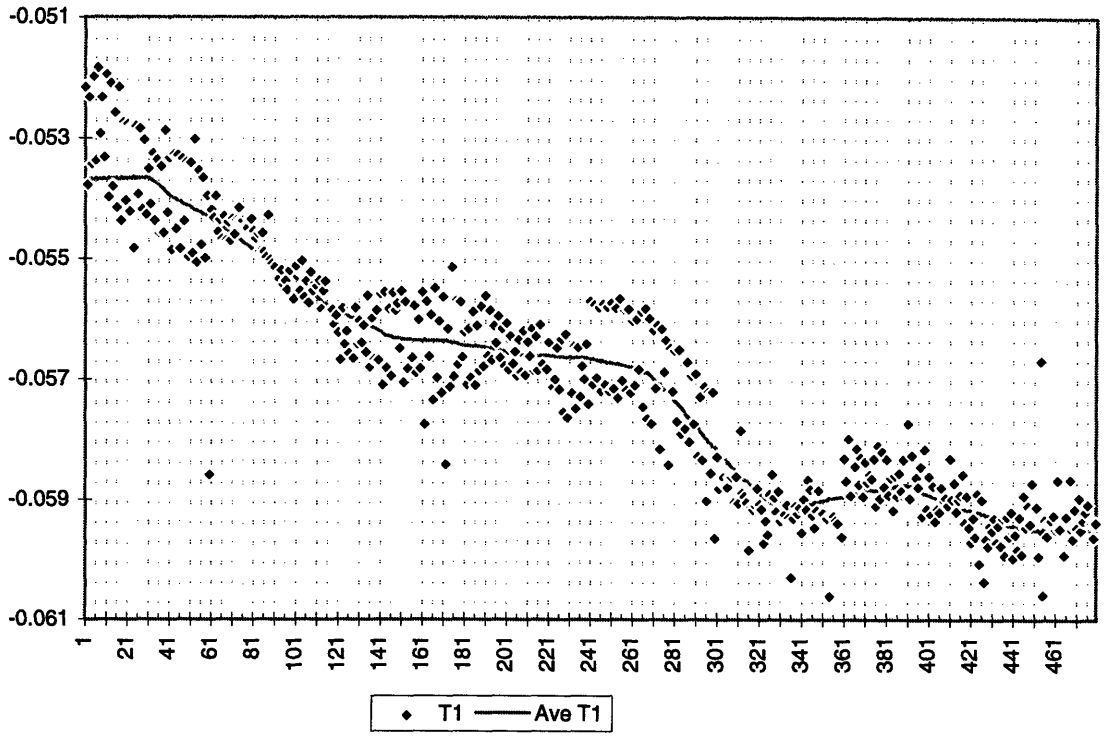

Figure 4-1: Response in volts vs. channel number of an FPA to T_1 immediately following cool–down.

minutes have passed. The approximately 10 minutes prior to starting measurements were spent cooling the dewar enough that the liquid nitrogen did not boil off as soon as it was poured. This agrees very well with the predicted 40 minute cool–down time.

Testing PCU on previous, smaller focal planes, failures at low temperatures rarely appeared.[2] Since smaller focal planes use a different test dewar than these larger ones, a plausible explanation is that the larger, "hockey–puck," dewars used in this thesis take much longer to stabilize in temperature than the smaller, more conventional, test dewars. The precise determination of the cause is not critical, since the flight dewars are not ever "warmed up." Waiting long enough for the FPA temperature to stabilize is only important when using the test dewars for "screening" FPAs before packaging them for use in the field.

4.1.3 Errant Pixels

An important consideration in improving PCU results is the removal of gross failures prior to commencing the PCU calculations. Since PCU failures are determined by comparing the

[2]Personal communications with test engineers, Donald Grays and Joseph Czapski, Lockheed Martin IR Imaging System, Lexington, MA.

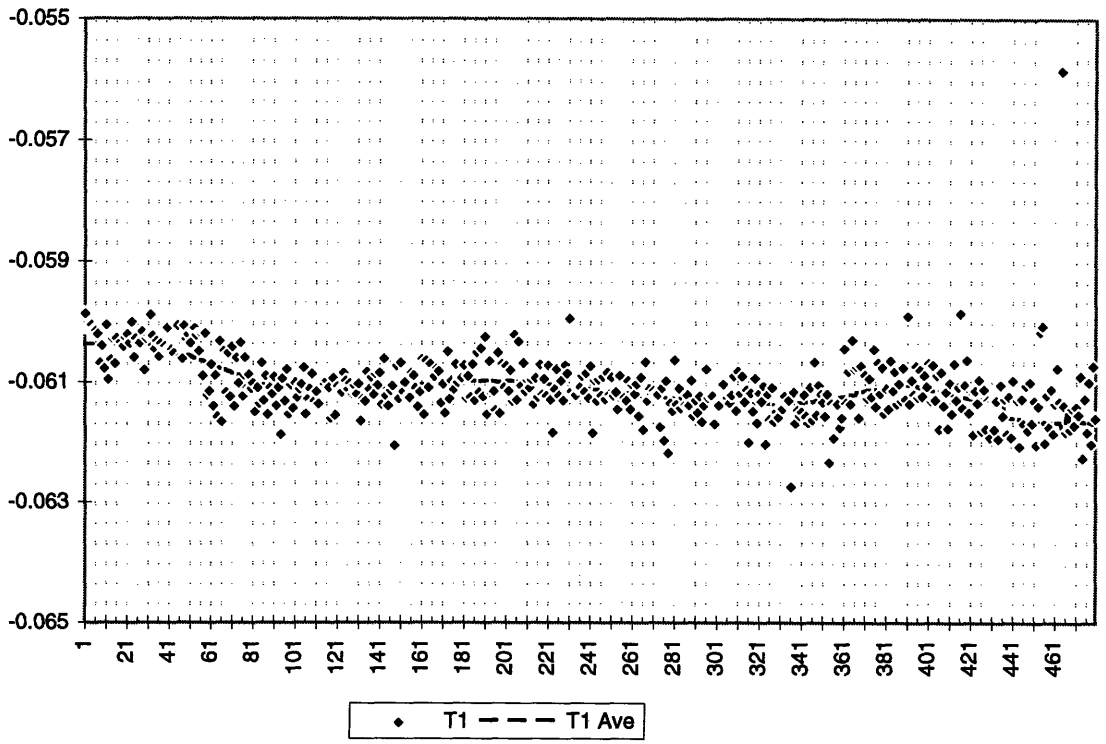

Figure 4-2: Response of the same FPA as shown in previous figure to T_1 90 minutes after initial cool–down.

results of one channel to the average of its nearest neighbors (see Eq. 3.4), it is important that grossly failing pixels do not cause "good" pixels to be labeled as failures by skewing the average significantly. An example of how this works is shown in Figures 4-4 and 4-5.

Figure 4-4 shows a moving average across an FPA. Notice that at the end of the array, the average "jumps." Pixels whose response is very close to previous pixels' begin to fail. The sudden increase in the average response is caused by a single (or several), errant pixel(s). The effect of deleting this pixel from all averaging results is shown in Figure 4-5. The average is now a much more constant value, and many fewer pixels fail. This illustrates how grossly failing pixels can significantly affect PCU calculations, and thus should be identified and eliminated prior to beginning PCU determinations.

4.2 FPA PCU Results

Five FPAs were tested and analyzed multiple times in detail. The summary of the PCU results is given in Table 4.2. Notice the high degree of repeatability in the number of failures at specific temperatures for specific focal planes. This is strong evidence that PCU failures

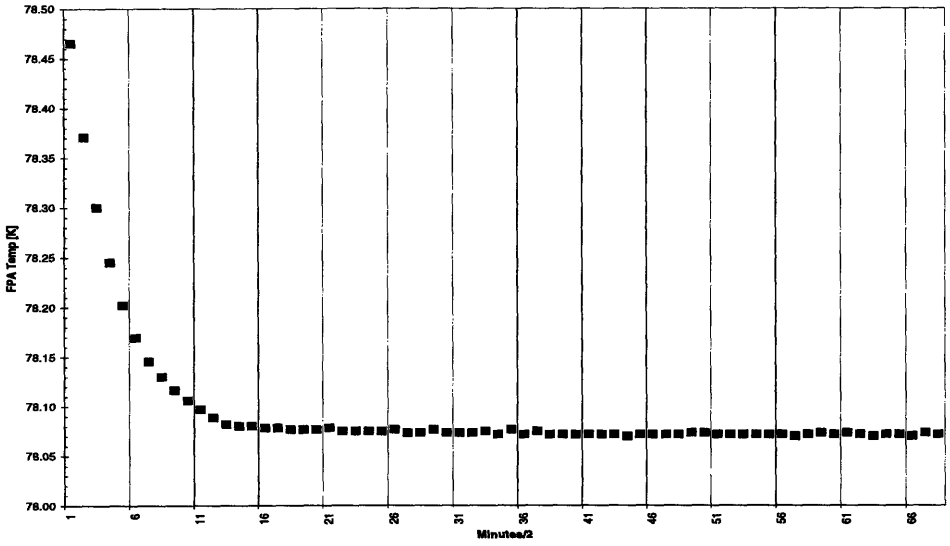

Figure 4-3: Focal plane temperature drift vs. time

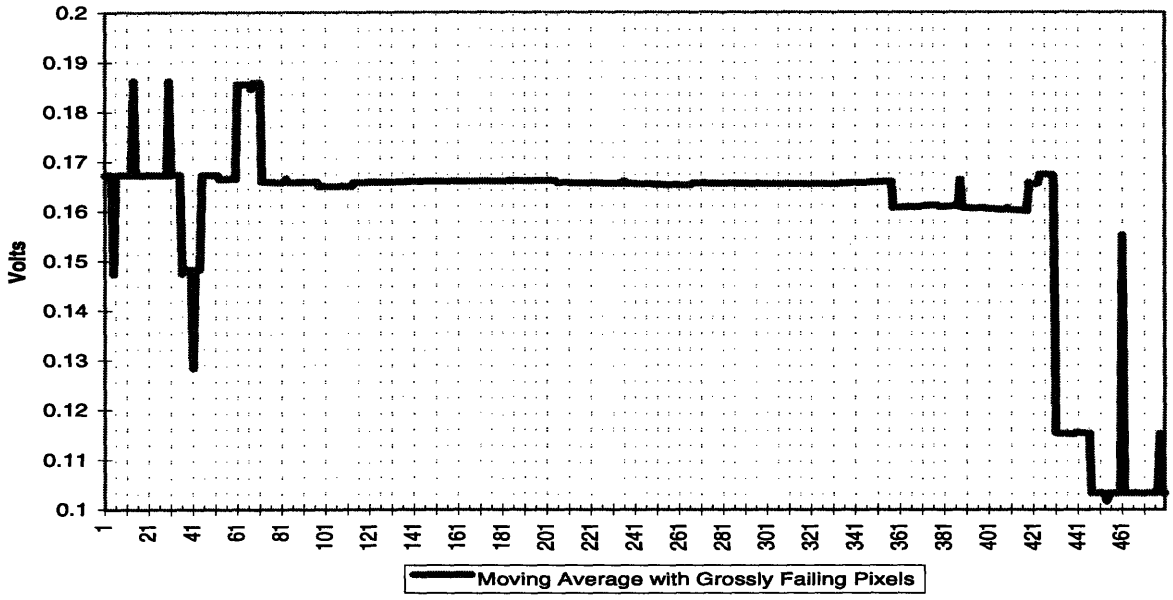

Figure 4-4: Plot of moving average with errant pixels included.

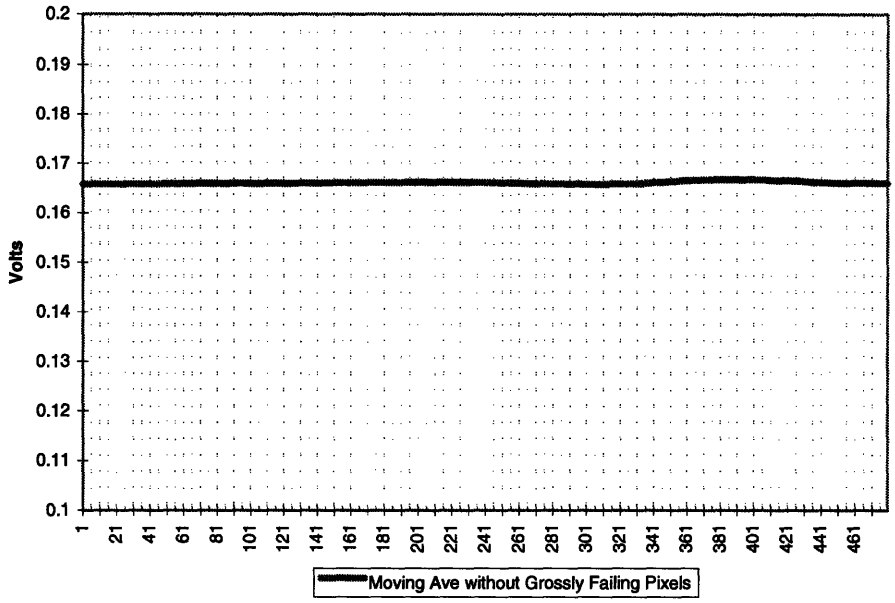

Figure 4-5: Plot of moving average with errant pixels excluded.

are not due to temporal noise effects. Some tests were eliminated from further analysis (and are not presented here) due to FPA temperature stability problems and/or test equipment failures.

Included in this table are the number of failures in DC Offset and Response to illustrate the consistency of most FPAs results. FPAs with few "bad" channels are especially good. Note also that tests run closely in time to one another display very good consistency of results.

A sample plot of PCU results at all four temperatures is shown in Figure 4-6. The rest of the PCU results for four different focal planes are included in Appendix A. The plot shows $V_{ce}(i, T_x)$, as defined in Section 3.5, for all four PCU temperatures for every channel i. In other words, $V_{ce}(i, T_x)$ is the difference in voltage between channel i and the average of its sixty nearest neighbors at one of the specified PCU temperatures. The voltage axis uses a grid spacing of $Vn = 830\mu V$ to enable easy determination of "failures" as defined by SADA. Ideally, if no post–correction nonuniformity (PCNU) existed on the FPA, these plots would be straight lines at 0. Analysis and discussion of the PCU data are included in the following chapter.

Table 4.2: Results summary table, giving number of failing channels out of 480.

ID Number		DC Offset	Response	Linearity	PCU			
FPA	**Test**				T_1	T_3	T_5	T_6
29	18.1807A	11	10	19	122	24	46	129
	18.1807B	11	10	16	164	26	41	129
	18.2109A	15	12	33	187	42	19	71
	18.2109B	11	10	16	166	27	41	**
	19.1724B	12	12	34	240	45	182	360
32	15.1619B	6	2	7	123	30	46	92
	15.1830A	6	2	7	131	34	51	104
	15.1830B	6	2	7	123	30	45	91
	21.2336A	6	1	8	160	29	69	131
	21.2336B	6	1	6	177	38	74	139
26	10.1147	8	23	480	378	7	**	**
	19.1127B	14	22	39	235	72	216	**
	18.2226B	23	24	36	186	118	150	257
25	10.1840B	7	23	480	11	4	3	35
	10.2212A	7	24	480	30	9	21	68
	10.2212B	7	24	480	9	4	3	8

ID $\equiv$ day.time of test, e.g. ID = 06.0123 would be day 6, 1:23 am. A and B indicate that 2 tests were run back–to–back.

* indicates that either the data are unavailable or that the number of failures is over 400.

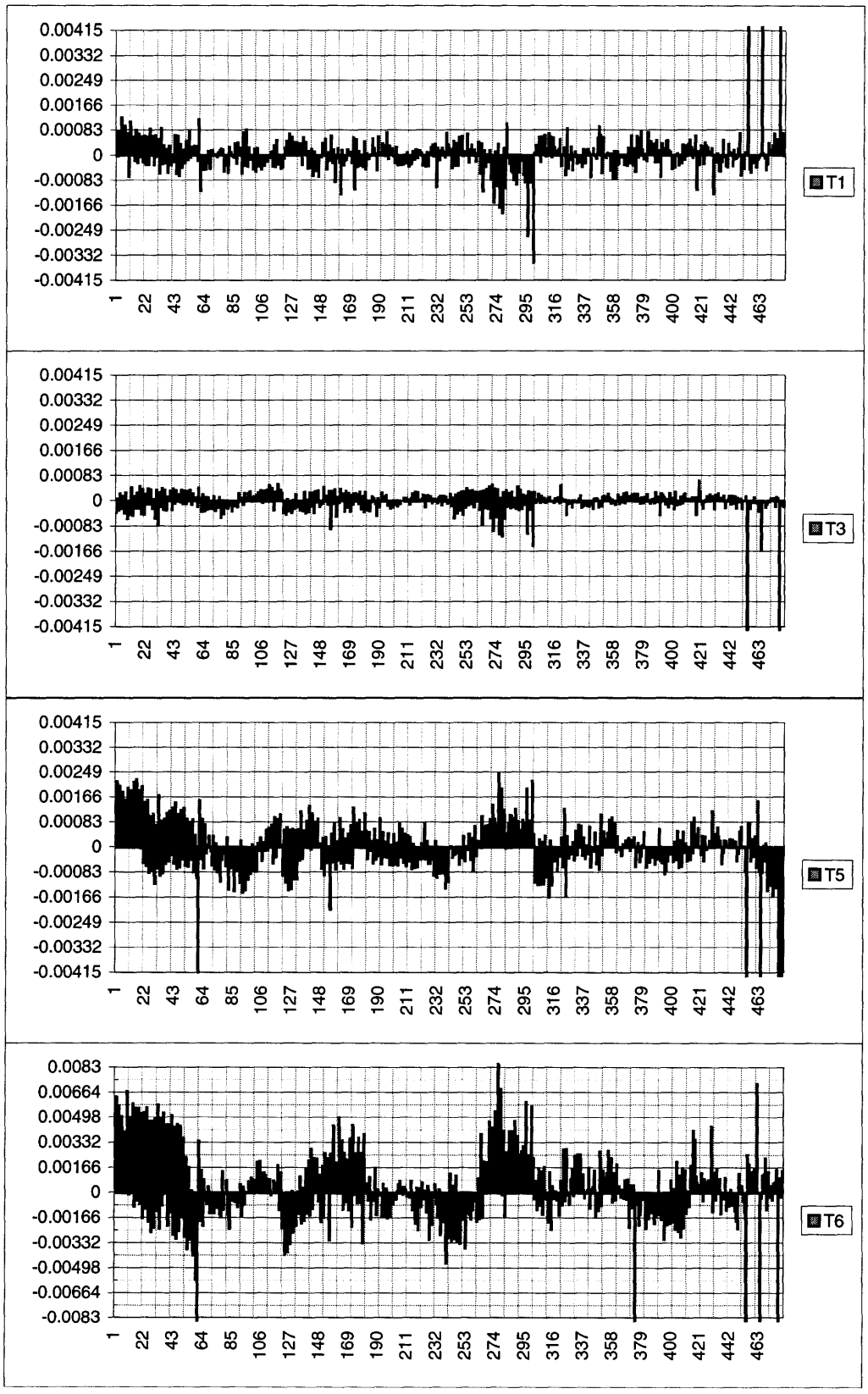

Figure 4-6: PCU results for all 6 temperatures on FPA 25 [Test ID: 102212a]. The vertical axis is volts; the horizontal is channel number.

Chapter 5

Analysis of Experimental Results

5.1 ROIC Contributions

5.1.1 Signal Chain

The signal chain of the ROIC describes the path that current generated in a detector takes to its ultimate destination of a displayable voltage. Many different methods of achieving this are used by IC designers, who must make constant design trade–offs in picking which type of stages to use. A block diagram of the SADA II 1–clip signal chain is shown in Figure 5-1.

TDI Chain and Input Cell

The detectors are attached in a TDI chain, which has several advantages. A TDI input sums the current from several detectors on a number of parallel capacitors and then passes that voltage up the signal chain. By summing the signal from several detectors, the signal–to–noise ratio is increased. Also, if individual detectors fail or are inoperable, they can be deselected, and the remaining detectors in the output are used [1]. In the event that one or more pixels are deselected from the TDI chain, the outputs of the remaining functional detectors are integrated on fewer capacitors in the transimpedance stage that are scaled appropriately to keep the responses uniform. This TDI uses six detectors, with a minimum of three working to have an operative channel, so four different capacitors can be selected depending upon the number of working detectors in a single channel.

Connecting the detectors to the ROIC is a differential buffered–direct–injection (BDI)

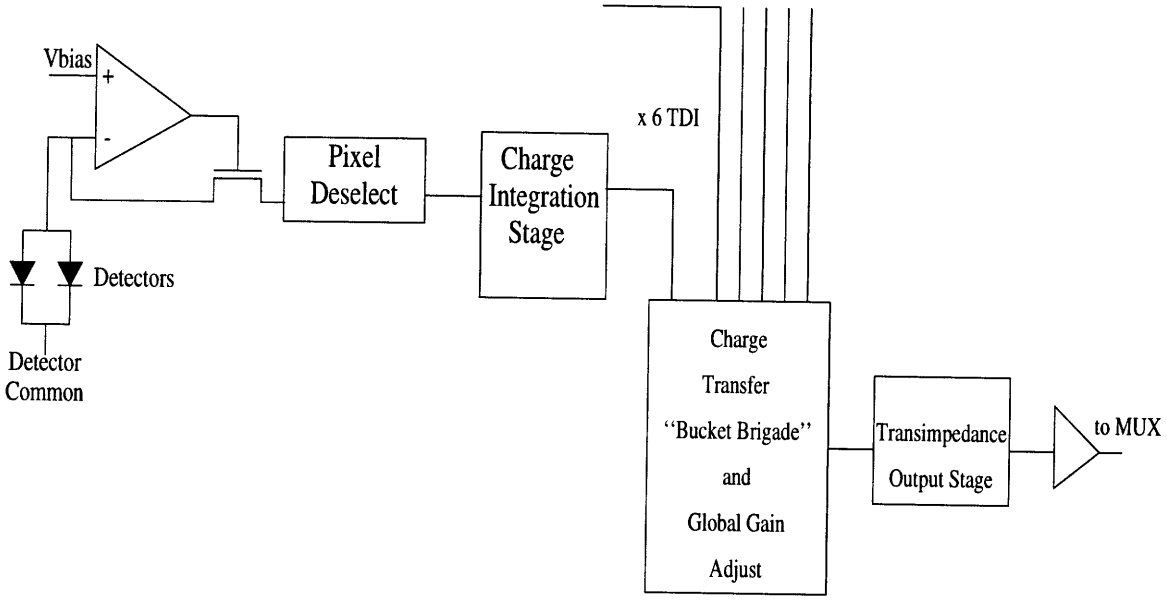

Figure 5-1: SADA II 1–clip signal chain block diagram.

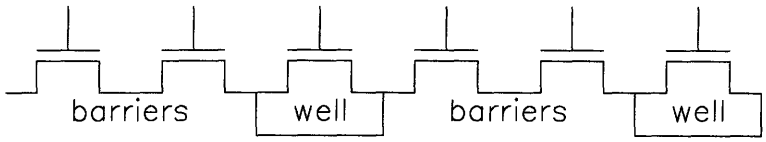

Figure 5-2: Schematic of two segments of the analog shift–register.

input coupling cell, which was chosen and implemented for its good detector bias control, coupling efficiency, and linearity, as well as low $1/f$ noise [8]. Following the BDI is a pixel deselect switch, which, when activated, shunts the current to ground, thus discriminating out the pixel.

If not shunted to ground, the current from each detector is integrated. The integration stage was designed to operate solely in the charge domain to increase linearity. Integration happens in two stages, on two n–well capacitors, which are reset to the same voltage after each integration period. This prevents charge on any parasitic capacitance from being passed down the signal chain by holding it the same with the voltage sources [8].

Analog Shift Register

After integrating the charge from each selected detector, the total charge from each channel must be summed. This happens by injecting the charge into a transfer shift–register that passes charge along the ROIC to the output transimpedance stage. The analog shift–register (shown in Figure 5-2) consists of alternating charge–holding "well" transistors and barrier "switch" transistors. Charge is accumulated in a "well" during a clock cycle and then "switched" into the next well, and on down the chain. Charge from each TDI stage is summed by transferring charge into this "bucket–brigade" shift–register at different points along the line. Thus, the first eight wells pass charge from the first detector, the second eight wells (eight are used due to the timing of the TDI and introduce the appropriate delay between detectors) pass charge from the first *and* second, etc.

The bucket–brigade is the first stage that is a potential significant source of error. The transfer efficiency of the wells in this "bucket brigade" is an important issue in design [8]. If the transfer efficiency is not very close to one, loss of charge can ensue, reducing the quality of the final image, as well as the overall performance. This is especially true if the transfer efficiency varies across the array.

Another way this stage can contribute to nonlinearity is a charge–overflow situation.

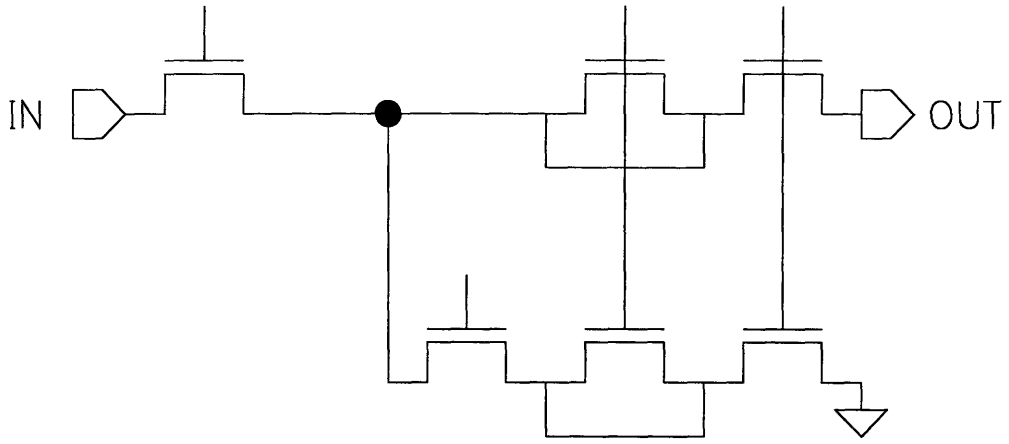

Figure 5-3: Schematic of SADA II 1–clip ROIC charge–splitting cell.

Inherent in the shift–register and crucial to its operation are limited capacity p–well capacitors. Although they have been sized to accommodate large amounts of charge, when viewing high scene–temperatures with all detectors selected, it is possible to "overflow" the capacity of one or several of these capacitors along the bucket–brigade [8]. This is a plausible and likely explanation for two results observed on many FPAs, indicated in Table 4.2: a nonlinearity over 5% and the high number of PCU failures at T_6.[1] Depending upon the responsivity of the detectors and the number deselected, the extent of this "overflow" phenomenon will vary from channel–to–channel.

Charge–Splitting Stage

The next step is a charge–splitting stage (global gain adjust) at the end of the shift–register. This is shown in Figure 5-3 The gain state allows the selection of the global gain states of 1/2, 1/3, and 1/6 required by the SADA specification. The nominal gain state is 1/3 [20]. The charge–splitting is accomplished by splitting the charge over a pair of n–well capacitors and then shunting the second to ground.

Many difficulties were encountered in designing the charge–splitting cell. It was discovered on previous designs that unless the capacitances of the two n–wells were identically matched, with no parasitics hanging on the splitting node, an uneven split occurred, par-

[1]This phenomenon of "roll–off" at high scene temperatures has only recently been observed in testing SADA ROICs. Dr. Frank Jaworski, a senior design engineer at Lockheed Martin IR Imaging Systems, Lexington, MA, contributed to this explanation of the effect in personal communications.

ticularly at low charge levels. After some detailed testing, a better cell was designed, and used here, with compensation for modeled parasitics [8].

Output Transimpedance Stage and Multiplexer

The final stage in the signal chain is the output transimpedance stage (Figure 5-4). It is here that charge is converted to voltage, and the signals are read out of the channels. Charge is converted to voltage on a combination of six parallel capacitors. The selection of which capacitors are used is determined by the global gain state and the discrimination pattern for a particular channel. Recall that These capacitors are voltage–dependent.

This stage has several inherent nonuniform non–linearities. One is processing variations that cause small, but unpredictable, capacitance differences through nonuniform ion implantation. The different discrimination patterns select differing capacitances, as described in Chapter 3. The different gains from detector deselect combined with varying capacitance from processing create nonlinearities that vary from channel–to–channel. Processing variations can also cause variations in the threshold voltages of the transistors, altering their $i - v$ characteristics, as well as their capacitance.

Also, the circuitry of this stage has some inherent nonlinearities, such as a reduced signal swing due to the floating switch on the signal side of the capacitor. The output stage was predicted to be the most nonlinear stage of the chain. This is due to the fact that conversion from charge to voltage is nonlinear because of the voltage–dependent characteristics of the capacitors [8]. The influence of non–linear capacitance on PCU is discussed more in following sections.

The output stage is connected to a 30:1 multiplexer. Most of the design issues in the multiplexer relate to settling times and will not be examined here.

A schematic of the layout architecture for the FPA is shown in Figure 5-5. Notice that, not only are the odd and even channels separate, the distance between the final stages is quite large—several hundred millimeters. This distance increases the liklihood that variations between odd and even outputs could occur.

5.1.2 Visual Evidence

Although PCU results in this work (the plots on pages 65— 74 in Appendix A) display variations in number of failures and "shape" of errors, some striking similarities appear.

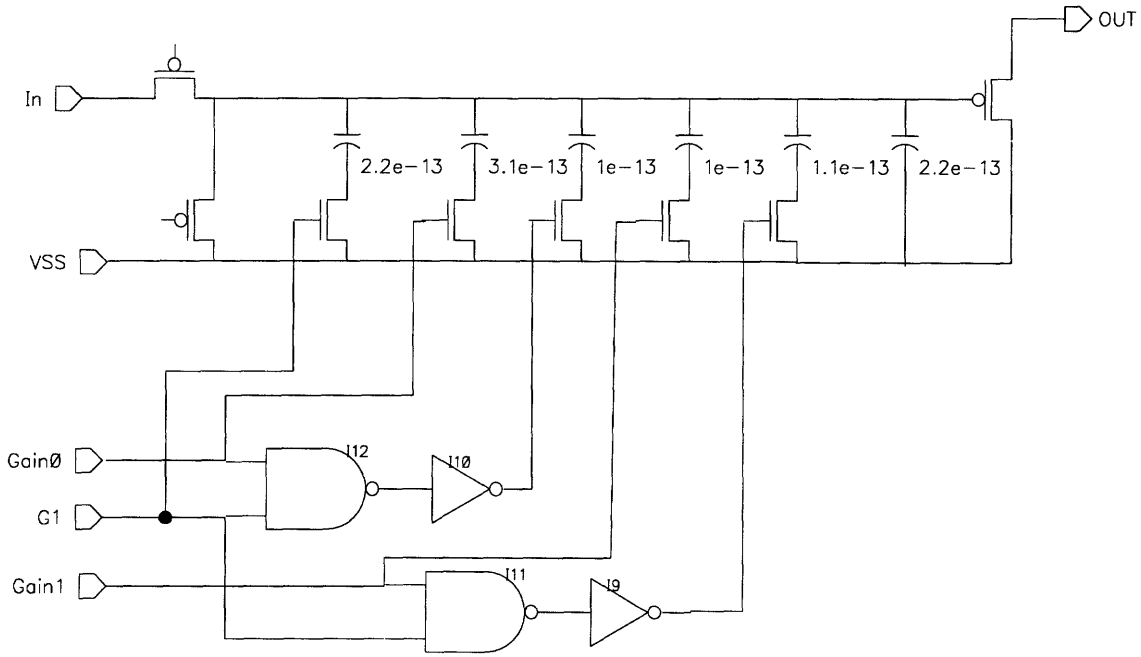

Figure 5-4: Schematic of SADA II 1–clip ROIC transimpedance output stage.

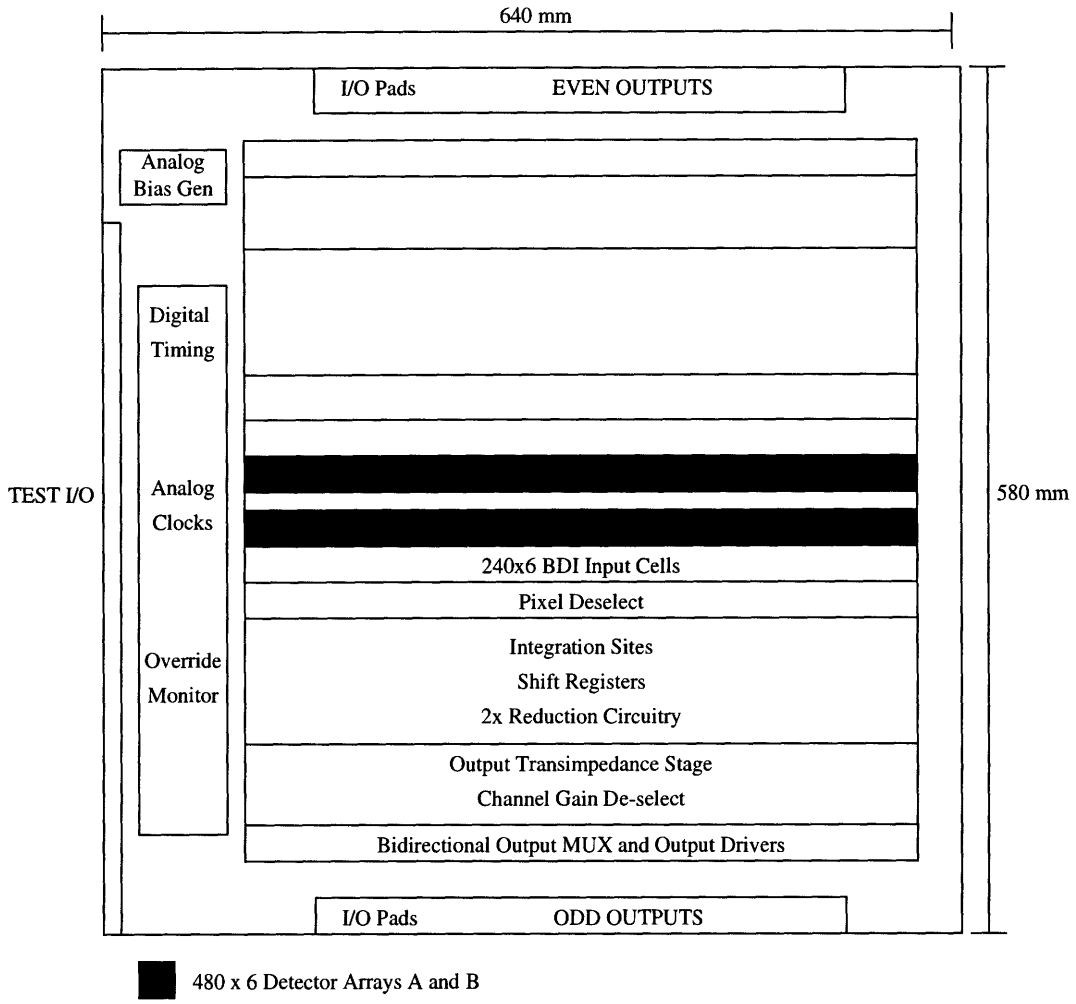

Figure 5-5: SADA IRFPA architecture layout.

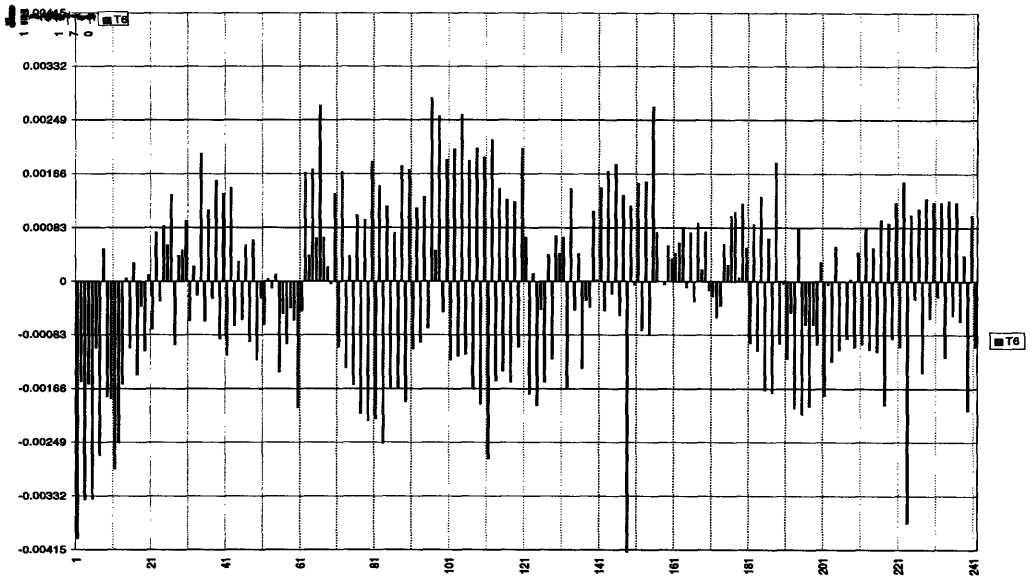

Figure 5-6: Example of an FPA PCU response at T_6 showing distinct odd/even and 60–channnel patterns.

The most significant of these is the alternating odd/even–channel response across the FPA. This appears at every temperature for every FPA. This effect can be due to only one thing: the ROIC. An example of this is shown in Figure 5-6. Recalling that the ROIC is laid out with even channels on one side and odd channels on the other, one would expect to see an odd/even–channel dependence if the ROIC was dominating the response. Contrarily, the detector array is linearly laid out, starting with channel 1 at one edge of the array and stepping across to channel 480 at the other side. Thus, any effects from the detectors would most likely appear as a gradient independent of odd/even affects. Further evidence of this is garnered by calculating PCU results using only odd or even channels. Doing so lowered the number of failures by 15% — 40% at various temperatures. A probable explanantion of this is the fact that, not only are the even and odd channels physically distant from one another, they do not share the same reference voltage wires. Instead, each half has its own reference voltages. Variations in the resistance of this wire, or even milliVolts of change from one reference to the other would result in the odd/even dependence seen here.

A second significant pattern involves "groups" of adjacent channels. This grouping is related to the layout of the ROIC output mux. As described above, after traversing

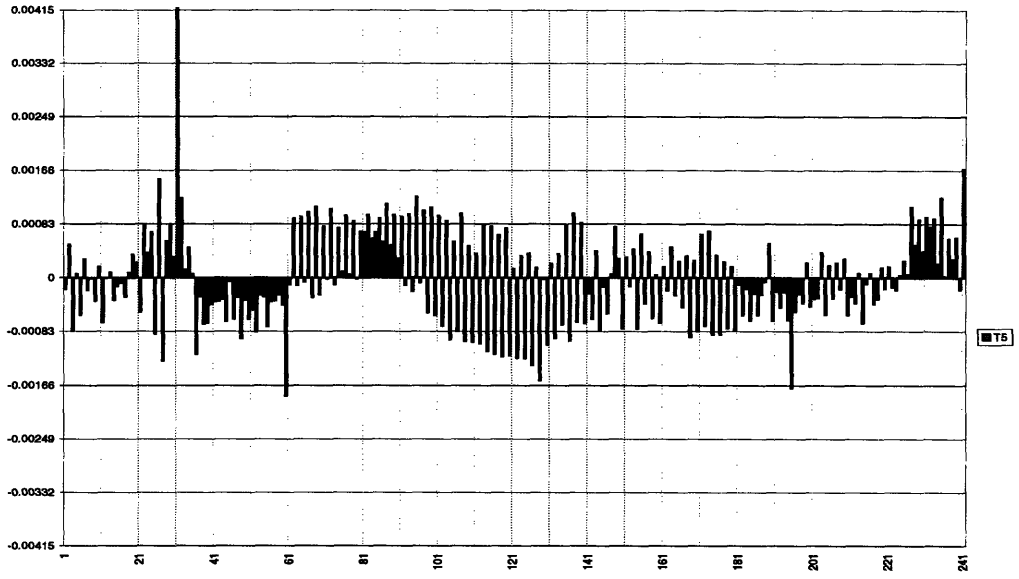

Figure 5-7: Example of FPA PCU repsonse showing 60–channel and odd/even patterns.

the entire signal chain, the channels are multiplexed 30:1 via sixteen multiplexors. So, channels 1,3,5,7,...,59, channels 2,4,6,...,60, and channels 461,463,465,...,479 each share a single output. The observed "groupings" of PCU results almost always correspond to a group of 60 channels, or two outputs (see Figure 5-7). Within these groups almost always appears the even/odd oscillation as well. If this grouping was due to the detectors, one would expect to see a smooth (no even/odd dependence) pattern independent of channel number. Nowhere does a pattern that fits that description appear.

The next thing to examine is what characteristics of the ROIC is causing these errors. The odd/even oscillations logically can be assumed to be due to some vertical variation in the FPA (outputs horizontally connected respond similarly), while the sixty channel groups are due to variations in the output muxes. In light of these results, the next questions to address are what is varying and why is it influencing PCU?

5.1.3 Output Transimpedance Stage's Capacitance

As mentioned in Chapter 1, the output stage of the ROIC is where the most nonlinearity is likely to occur. The output transimpedance stage is where the charge becomes converted

to a voltage. A schematic was shown in Figure 5-4. One of the clear causes of nonlinearities in this stage is the number of capacitors involved.

Capacitors in complementary metal–oxide–semiconductor (CMOS) technology are usually made from glass, which makes a nearly ideal capacitor with no leakage current or shunt resistance. These are very linear. Unfortunately, the silicon amplifiers and switches, which these glass capacitors are attached to, do not display such linear characteristics. Thus, they add nonlinear parasitic capacitance to the (formerly) ideal glass capacitor. The resulting transfer characteristic therefore causes a nonlinear output [6].

Nonlinear, voltage–dependent capacitance can be described as follows:

$$C(V) = C_a + \frac{C_p}{\sqrt{1 + V/V_\phi}} \tag{5.1}$$

with C_a as the "actual capacitance" from the linear, glass capacitors, C_p is the parasitic, voltage–dependent capacitance, and V_ϕ is the built–in potential of the CMOS transistors ($\sim 1V$) [6]. This V_ϕ often varies with processing as well. Variations in V_ϕ can affect the parasitic capacitance of the switches.

In order to relate this capacitance to actual ROIC parameters, one needs to relate the capacitance to the current flowing into the ROIC from the detectors, I_o. That can be expressed as follows:

$$I(t) = \frac{dQ}{dt} = C\frac{dV}{dt} + V\frac{dC}{dt} \tag{5.2}$$

Integrating both sides of Equation 5.2 gives

$$\int_0^{t_i} I_o dt = \int_0^{V_o} \left(C_a + \frac{C_p}{\sqrt{1 + V/V_\phi}} - \frac{V}{2V_\phi}\frac{C_p}{\sqrt{(1 + V/V_\phi)^3}} \right) dV \tag{5.3}$$

where t_i is the integration time, and V_o is the output voltage. Performing the integration, the non–linear relation for the output voltage is given by

$$V_o = \frac{I_o t}{C_a + \frac{C_p}{\sqrt{1+V_o/V_\phi}}} = \frac{I_o t}{C_{eff}(V_o)}. \tag{5.4}$$

On SADA II 1–clip ROICs, the modeled effective capacitance, $C_{eff}(0) = C_a + C_p$, for a TDI of six and a global gain of one is $0.84pF$. Experimental results did not give this same

value; this is discussed below.

It becomes clear from this that even small variances in capacitances (probably caused by V_ϕ variations) will affect the linearity of the output voltage. This is particularly true if I_o varies as well. Assuming uncorrelated fluctuations in C_{eff} and I_o, a simple error propagation calculation yields [3]:

$$\frac{\Delta V_o}{V_o} = \sqrt{(\frac{\Delta C_{eff}}{C_{eff}})^2 + (\frac{\Delta I_0}{I_0})^2}, \tag{5.5}$$

where

$$\frac{\Delta C_{eff}}{C_{eff}} = \sqrt{\frac{(\Delta V_o)^2}{2V_\phi}(1 + V_o/V_\phi)^{3/2}}. \tag{5.6}$$

Even if C_{eff} were not dependent on voltage, as the ROIC designers would like, Equation 5.5 shows how variations in C_{eff} and I_0 nonlinearly cause variations in V_o.

The final output stage of the ROIC selects integration capacitors based upon the gain state and the number of selected detectors in the channel. The size of these capacitors was designed to make the outputs of every channel uniform no matter how many detectors (3 – 6) were selected in it. This adds to possible gain variations.

The results from the two linearity tests described in Chapter 3 were used to calculate integration capacitance. Because the exact value of the initial integration capacitor is not known, neither of them can provide the precise value of C_{eff}; they only can determine precise ratios and/or precise variances in absolute values. Fortunately, for correctability purposes, this is all that is necesary. The most important values are comparative; that is, how much the values and ratios vary from channel to channel.

The variance in C_{eff} becomes important in order to calculate its impact on V_o. Table 5.1 lists the standard deviation (square root of variance), σ, of C_{eff} for the three wafers tested, all deselect patterns and gain state 3.

Table 5.1: Average value and standard deviation of capacitance [pF] across several ROICs.

WAFER	6 DETECTORS		5 DETECTORS		4 DETECTORS		3 DETECTORS	
	Ave.	σ	**Ave.**	σ	**Ave.**	σ	**Ave.**	σ
12	3.13	0.09	2.33	0.45	1.66	0.11	0.93	0.04
10	2.24	0.28	1.60	0.76	1.06	0.51	0.59	0.28
DVT	2.94	0.02	2.04	0.20	1.35	0.14	0.76	0.08

Using experimentally–determined values of ΔC_{eff} and ΔV_o, it is possible to calculate the variance in I_0 needed for this analysis. By picking a range of values, a range of 5–15 nA variation in detector current was calulated to cause the observed errors in V_o, and consequently PCU. Since V_o and V_c are linearly related, the error propagation is simply $\Delta V_o/V_o = \Delta V_c/V_c$ [3]. Variations on the order of 10 nA are not unreasonable across an array.

5.2 Correlation Between Detector Parameters and PCU

In searching for causes of poor uniformity among so many variables, it is useful to eliminate some parameters as not significantly affecting the results. One approach is to plot variables pairwise looking for correlations. With large amounts of data and/or pairs to be considered, this method becomes overly time–consuming. A more appropriate technique is to use a correlation coefficient matrix.

A correlation coefficient is a measure of the covariance of two variables. In simple terms, it measures how well a pair of variables correlate. The covariance, $\sigma^2_{x,y}$, of two variables, x, y, on which correlation is based, is calculated by:

$$\sigma^2_{x,y} = \frac{1}{n}\sum_{j=1}^{n}(x_j - \langle x\rangle)(y_j - \langle y\rangle) \tag{5.7}$$

where n is the number of "samples" of the variables x, y; and $\langle x\rangle$ is the mean value of x. This value, $\sigma^2_{x,y}$ must be normalized by the variances of the individual variables to give useful information. Consider, for example, two variables, x, y, as having Gaussian distributions. In calculating the variance, the mean of both variables shifts to 0 by subtracting their individual averages. Then, dividing by the standard deviation of each sets each variable's "width" to 1. This makes evaluating their linear correlation possible. Thus, normalizing Equation 5.7 by the covariances of the individual variables gives the linear correlation coefficient:

$$\rho_{x,y} = \frac{\sigma^2_{x,y}}{\sigma_x \sigma_y}, \tag{5.8}$$

where $\sigma^2_x = \sigma^2_{x,x}$. The value $\rho_{x,y}$ then represents the degree to which variables x and y are linearly correlated [3, 19].

For $|\rho|$ close to one, a good correlation between the variables exists; for values close to

zero, little or no correlation exists. (The maximum value $|\rho|$ can take is 1.) A quantitative evaluation of the confidence level associated with a given value of ρ can be determined from the integrated probability distribution [3, 19].

Table 5.2 gives the probability, $\mathcal{P}_n(\rho_o)$, that n values of two uncorrelated variables would have a correlation coefficient, $\geq \rho_o$. If $\mathcal{P}_n \leq 1\%$ the correlation is considered "highly significant," $\mathcal{P}_n \leq 5\%$ indicates "signifcant" correlation [19]. As n increases, the magnitude of ρ needed to show correlation decreases significantly. For example, when $n = 10$, a 78% chance exists that no correlation will yield a $\rho = 0.3$, but when n increases to 100, only a 0.2% chance exists that ρ will equal 0.3 [3, 19]. In determining correlations of variables for FPAs, $n = 480$, the number of channels.

Table 5.2: Probability of correlation for certain values of correlation coefficients.

ρ_o	0	0.025	0.050	0.075	0.100	0.125	0.150
$\mathcal{P}_{n=480}$	1	0.586	0.275	0.101	0.029	0.006	0.001

Having established a quantitative measurement of correlation between variables, the PCU data and measured characteristics of the detectors can be compared. One would expect to see large correlations between those factors significantly affecting PCU and post–correction voltages themselves. Several detector characteristics are routinely tested in screening detectors for discrimination, as well as screening FPAs for performance. These were compared and a large correlation coefficient matrix created (Table 5.3). Note that responsivity and quantum efficiency values is that responsivity is calculated prior to discriminating out "bad" diodes, while quantum efficiency is calculated using only selected diodes.

"Highly significant" correlation exists between $V_c(T_1)$ and $V_c(T_6)$ and D* and QE, quantum efficiency. "Significant" correlation appears between $V_c(T_1)$ and the other detector characteristics, offset and responsivity. No other detector parameter correlates at all with any FPA corrected voltage. This indicates that at T_3 and T_5 the detector parameters examined are not dominating, or even significantly affecting, PCU.

However, at T_1 and T_6, the small but significant correlation values show that detector parameters are impacting the PCU results at the outer temperatures. These values are not large enough (compare to values in Table 5.4) to indicate that quantum efficiency or D*

Table 5.3: Correlation coefficients for FPA corrected voltages and detector characteristics (params).

PARAMS	DETECTOR				FPA/ROIC			
	Offset	Resp	D*	QE	$V_c(T_1)$	$V_c(T_3)$	$V_c(T_5)$	$V_c(T_6)$
Offset	1.000							
Response	0.954	1.000						
D*	0.326	0.326	1.000					
QE	0.584	0.696	0.378	1.000				
$R_d(0V)$	-0.067	-0.056	-0.072		0.028	0.004	0.007	-0.014
$R_d(20V)$	-0.006	-0.028	0.039		-0.029	-0.002	0.020	0.005
$R_d(40V)$	0.014	-0.013	-0.040		-0.009	-0.013	0.008	-0.017
$V_c(T_1)$	-0.100	-0.102	-0.148	-0.140	1.000			
$V_c(T_3)$	0.030	0.009	0.028	-0.004	0.006	1.000		
$V_c(T_5)$	-0.039	-0.006	-0.012	0.011	0.816	-0.249	1.000	
$V_c(T_6)$	0.042	0.089	0.119	0.183	-0.070	-0.926	0.276	1.000

alone are dominating the results, but that part of the nonuniformity is due to QE and/or D* variations. This significant but weak correlation fits the earlier hypothesis (see Chapter 2) that a coupling between nonuniform detector parameters and nonlinearities in the ROIC could be causing the PCNU.

To further illustrate the point that detectors are either not correlating at all or only weakly correlating, Figure 5-8 contains $x - y$ plots of several detector parameters *vs.* FPA PCU voltages. Only flat lines or "scatter" patterns are seen, even at T_6. Similar results were observed on several FPAs. The lack of visible, graphical correlation is not inconsistent with the relatively low correlation values.

Seeing weak or no correlation between FPA corrected voltages and detector parameters does not imply the detectors are not affecting the output of an FPA. On the contrary, the detector may very significantly affect the uncorrected output or even dominate the uncorrected output and still, with no loss of consistency, lack correlation with outputs after correction. That lack merely implies that the variations in detectors are linear "errors" that disappear when the outputs are normalized and linearized in the PCU calculations.

Table 5.4 shows the correlations coefficients between the same detector parameters and voltages corrected only for offset, not gain. "Highly significant" correlations appear more often in this matrix, most noticeably on $V_o(T_6)$. This indicates that multiplicative "errors" from the detectors correlate with outputs at higher scene–temperatures, but that the linear

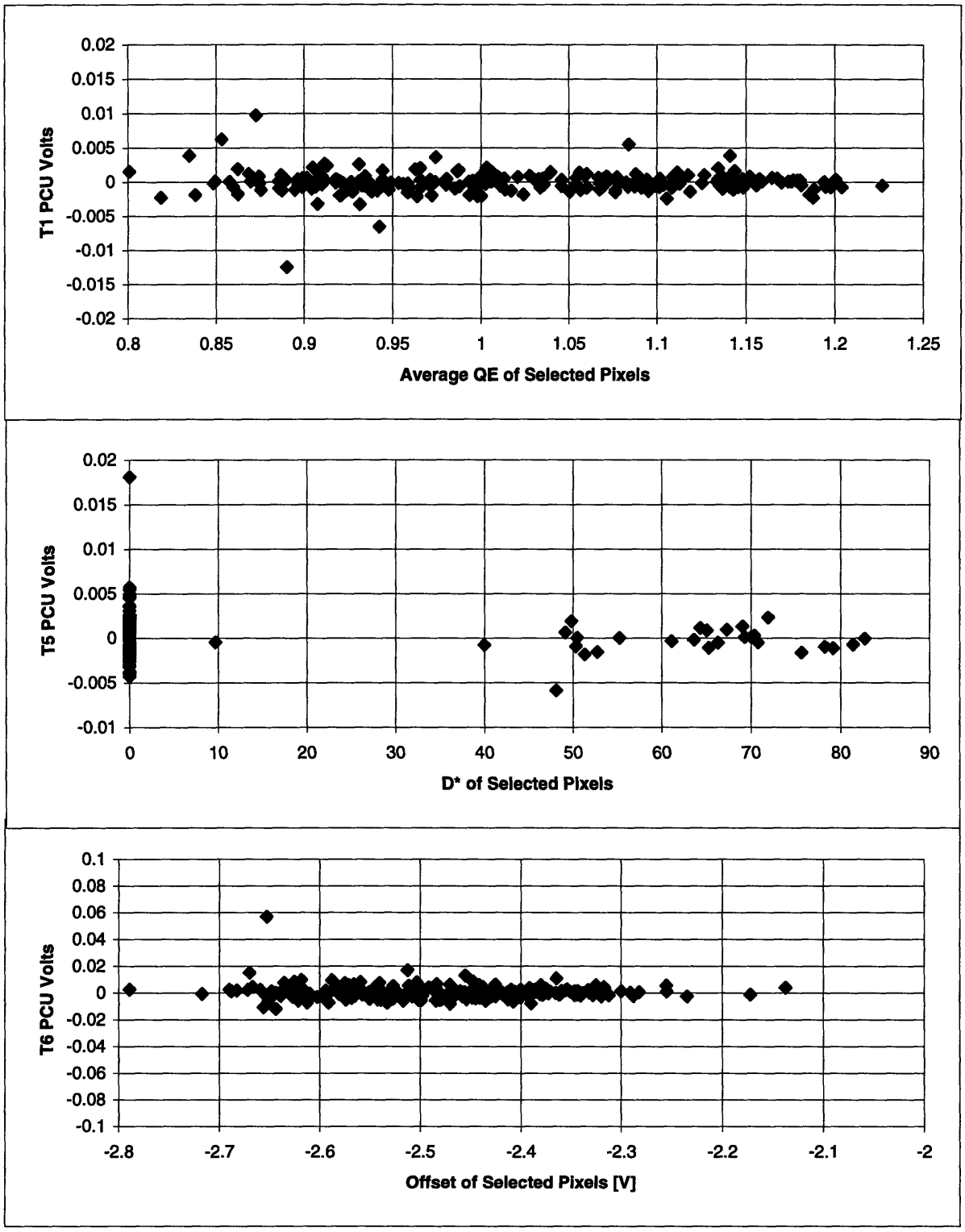

Figure 5-8: Plots of some detector characteristics *vs.* FPA PCU voltages.

PCU correction scheme is working to eliminate those variations, although not entirely.

Table 5.4: Correlation coefficients for FPA partially corrected voltages and detector characteristics.

PARAMETERS	DETECTOR			FPA/ROIC				
	Offset	Resp	D*	Gain	$V_o(T_1)$	$V_o(T_3)$	$V_o(T_4)$	$V_o(T_5)$
Response	0.954	1.000						
D*	0.326	0.326	1.000					
Gain	-0.881	-0.852	-0.299	1.000				
$V_o(T_1)$	-0.055	-0.072	-0.018	-0.092	1.000			
$V_o(T_3)$	0.012	0.029	-0.004	0.136	-0.999	1.000		
$V_o(T_4)$	0.054	0.071	0.017	0.093	-1.000	0.999	1.000	
$V_o(T_5)$	0.132	0.150	0.057	0.007	-0.990	0.985	0.991	1.000
$V_o(T_6)$	0.322	0.337	0.162	-0.189	-0.952	0.936	0.952	0.972

5.3 FPA Temporal Noise

Schulz and Caldwell discussed a Gaussian ($\Gamma(x)$) estimation of the temporal noise of an FPA [16], using a well–known χ^2 analysis [3].

$$\chi_i^2 = \sum_{x=1}^{6} \frac{(V_c(i,T_x) - \langle V(T_x)\rangle)^2}{y_{tx}^2}, \tag{5.9}$$

where $\langle V\rangle$ is the mean value of V over all channels; $x = 1,...,6$ is the number of the blackbody temperatures used, $i = 1,...,480$ is the number of the channel, $V(i,T_x)$ indicates one of the values in the data set, y_{tx} is the mean temporal noise over the array at a single blackbody temperature. If the only noise source in a uniform (corrected) FPA is temporal noise, χ^2 has a Gaussian probability distribution [16].

To determine what contribution of the overall PCNU is due to temporal, such as $1/f$, noise in the FPA, and how much remaining PCNU, ε, needs to be explained by the other factors that influence it, it is necessary to calculate how the experimentally–produced χ^2 histogram differs from the ideal (Gaussian) one. Equation 5.10 does just that by subtracting one from the other (again, the denominator terms are due to degrees of freedom in the system):

$$\varepsilon = \sqrt{\frac{\sum_{i=1}^{480}\chi_i^2}{(480-1)(n-2)} - 1} = \sqrt{\frac{\sum_{i=1}^{480}\sum_{x=1}^{6}(V_o(i,T_x) - \langle V(T_x)\rangle)^2}{(480-1)(n-2)} - 1}. \tag{5.10}$$

Thus, when $\varepsilon = 0$, all error in the system is due to temporal noise, and, when $\varepsilon = 1$, the remaining error *not* due to temporal noise is equal to the error due to temporal noise. If $\varepsilon \gg 1$, the error contribution from temporal noise is insignificant compared to the error from other sources [16].

When considering responses at a particular T_x, Equation 5.10 can be further simplified to merely:

$$\varepsilon = \sqrt{\frac{\sum_{i=1}^{480}(V_o(i) - \langle V \rangle)^2}{y_t^2} - 1} = \sqrt{\frac{\sigma^2}{y_t^2} - 1} \tag{5.11}$$

where σ is the standard deviation of the responses from their mean value, and y_t is the temporal noise of the responses. Since σ comprises both temporal and other sources of error, if these are independent, $\sigma^2 = y_t^2 + \sigma_s^2 = \sigma(V(T_x))^2 + \sigma_s^2$, where σ_s is the noise from other sources only.

The values of ε were calculated for several test results on different FPAs. The "raw," uncorrected voltages are used for this calculation, because that is where the temporal noise would appear. The fact that the values are similar at all temperatures indicates that temporal noise does not contribute at any of the temperatures. Consistently, $\varepsilon \gg 1$, usually by an order of magnitude. This implies that temporal noise is not dominating PCNU. This conclusion is supported by the good degree of repeatability of results (see Table 4.2). Table 5.5 shows the values of epsilon for several temperatures.

Table 5.5: Average epsilon values for two FPAs at several temperatures.

FPA	T_1	T_2	T_3	T_4	T_5	T_6
25	8.7	8.8	8.7	8.8	8.9	9.0
13	10.5	10.5	10.5	10.5	10.5	10.5

Chapter 6

Conclusions and Recommendations

Uniformity is a necessary specification for good performance of IRFPAs. The need for fast, real-time correction of channel response in tactical and strategic applications necessitates using a linear correction scheme. The most common is a two-point correction, which, during each frame, calibrates the array to two set-temperatures. Unfortunately, nonlinear nonuniformities exist in all IRFPAs creating post-correction nonuniformities. Several possible contributions to these nonuniformities were examined.

6.1 Conclusions

Test parameters, such as blackbody temperature drift and stability of focal plane temperature, were examined first. It was determined, as discussed in Chapter 4, that focal plane temperature variations during testing were significantly impacting PCU results. This problem was corrected by both monitoring FPA temperature during testing, and waiting long enough for the temperature to stabilize before beginning PCU measurements. No other test parameters were found to influence PCU at all.

Temporal noise contributions, such as $1/f$ noise, were determined to be insignificant contributors. This is shown in two ways. The first is the high degree of repeatability of results, as displayed in Chapter 4 in Table 4.2. The second is by analyzing the expected amount of temporal noise in the system and then comparing it to the total variation in the system, as is described in Chapter 5.

Many detector characteristics, among them R_d, quantum efficiency, and responsivity, were considered and investigated. Correlation calculations and plots showed no significant impact from detector characteristics on corrected output voltages close to the calibrations points, though pre-correction response correlated well. Weak correlation with quantum efficiency appeared at temperatures farther from the calibration points. The alone does not explain all the PCNU, but clearly is contributing in part.

After remedying the testing impacts and eliminating detectors as contributors to PCNU, attention was focused on the ROIC. The PCU data indicate that some characteristic of the ROIC is significantly impacting post–correction response variations. This conclusion is supported by the typical variations in the channels of the ROIC, as well as the nonlinear, threshold–voltage dependence characteristic of the capacitance in the signal chain. The design of the ROIC attempted to emphasize linearity concerns, and succeeded in making the channel linear within specifications for linearity over most of the dynamic range. As discussed by Herzog [6], this is not sufficient to meet the PCU requirement. The theory of nonuniform, linear affects from detectors coupled to nonlinear effects characteristic of the ROIC is supported by these data.

Further determination of the exact cause of the PCNU is not possible, since the ROIC was fabricated with performance in mind, not diagnostic testing. This severely limits what parameters of the ROIC can be directly (or even indirectly) measured.

6.2 Further Work

Although significant progress towards improving PCU on high-performance long-wave infrared sensors was made, much remains to be investigated. The most important is examination of other IRFPAs. SADA II 1–clip was tested in detail for this thesis, but testing of other IRFPAs would enrich the body of knowledge on the subject.

A second area needing work is better models of the nonlinearities of ROICs. Several test chips using different critical signal path designs should be fabricated and profiled to aid in this. A careful analysis of the contributions of various stages of the signal chain, not only to linearity, which was modeled for this ROICs design, but to overall PCU is needed. Once the ROIC factors are addressed, it may be that the whole process of "tracking down" the limiting factors in PCU will need another iteration.

A third test that would provide valuable information is determining the spectral shapes of detectors and then observing whether a correlation to PCU exists. This test was not done here due to lack of time and resources, but the impact of spectral shape on photocurrent, particularly at low temperatures indicates that it could be a strong contributor to nonlinear nonuniformities.

Finally, a close examination of a particular ROIC and careful characterization of the detectors mounted to it, all prior to hybridizing, is necessary to model sufficiently the coupling effect between the nonuniformity of the detectors and the nonlinearity of the ROIC.

Appendix A

PCU Results

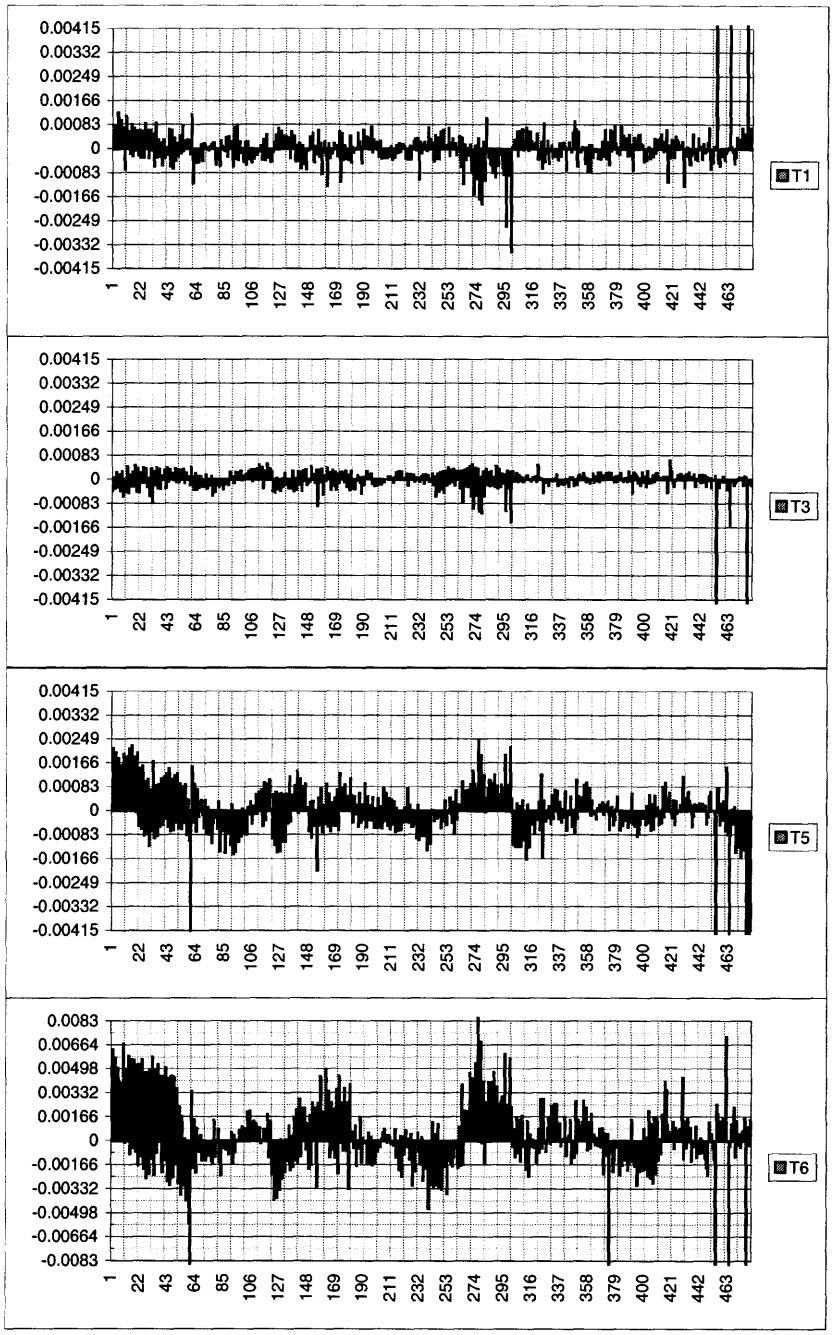

Figure A-1: PCU results for all 6 temperatures on FPA 25 [Test ID: 102212b].

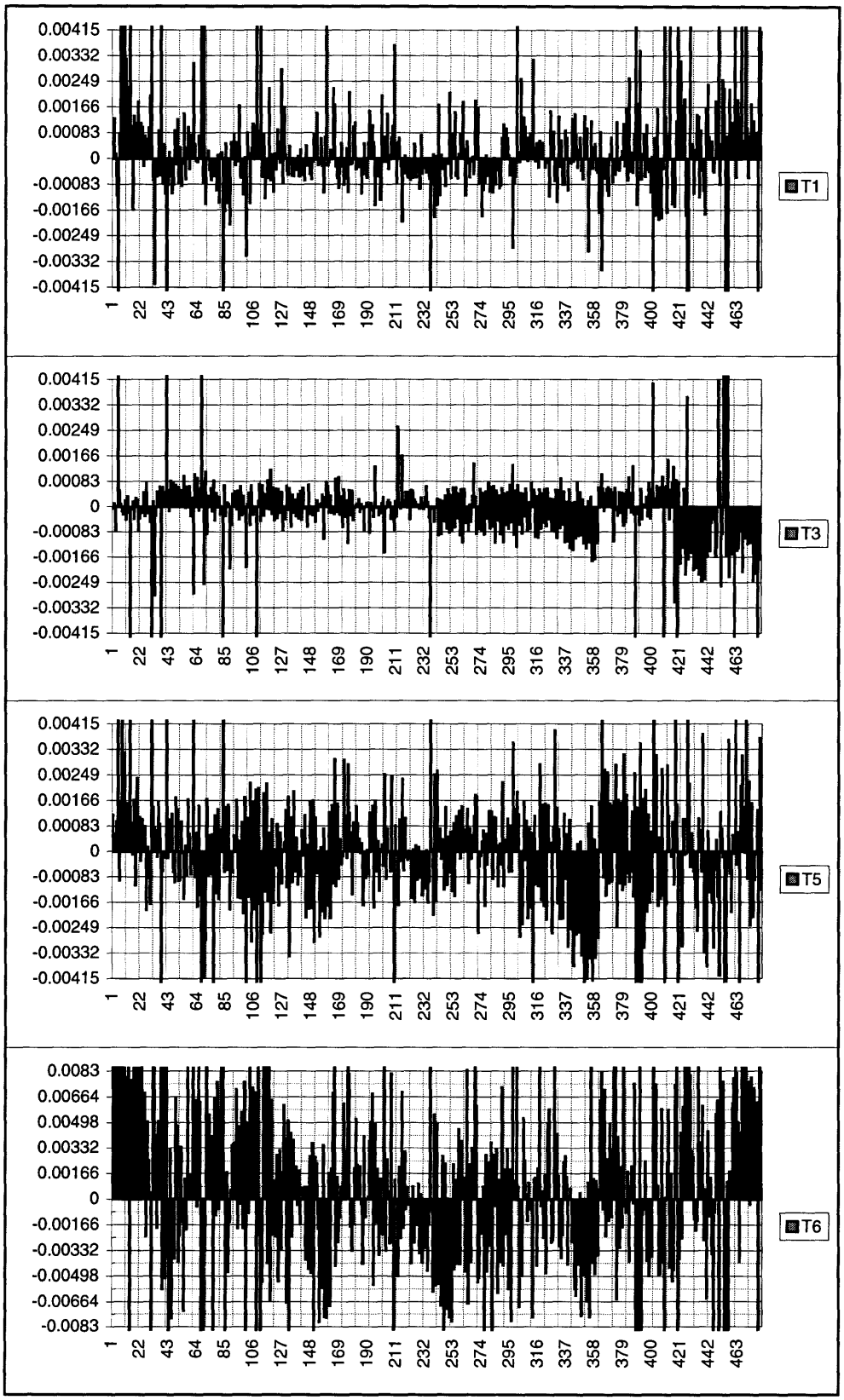

Figure A-2: PCU results for all 6 temperatures on FPA 26 [Test ID: 182226].

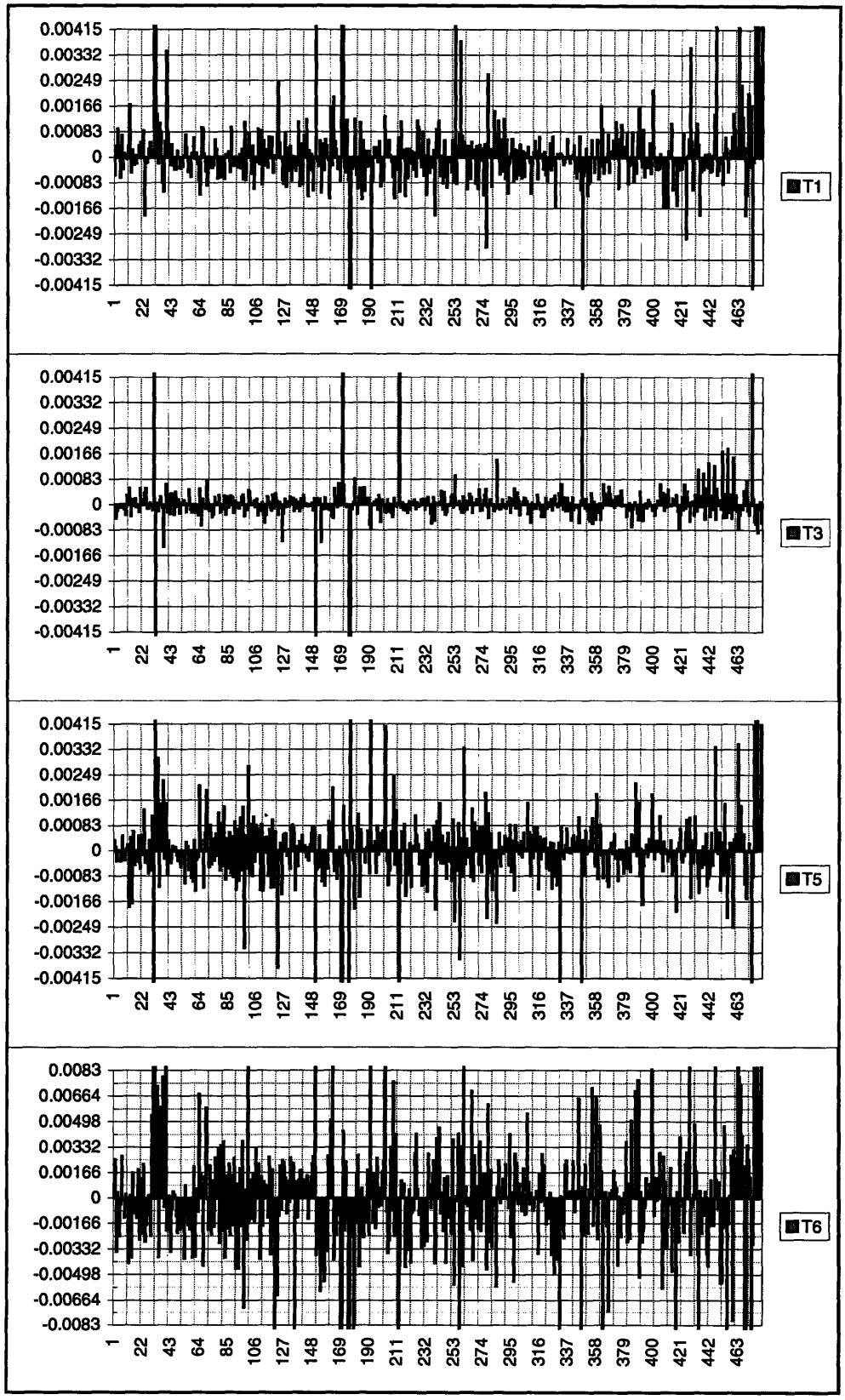

Figure A-3: PCU results for all 6 temperatures on FPA 29 [Test ID: 181807a].

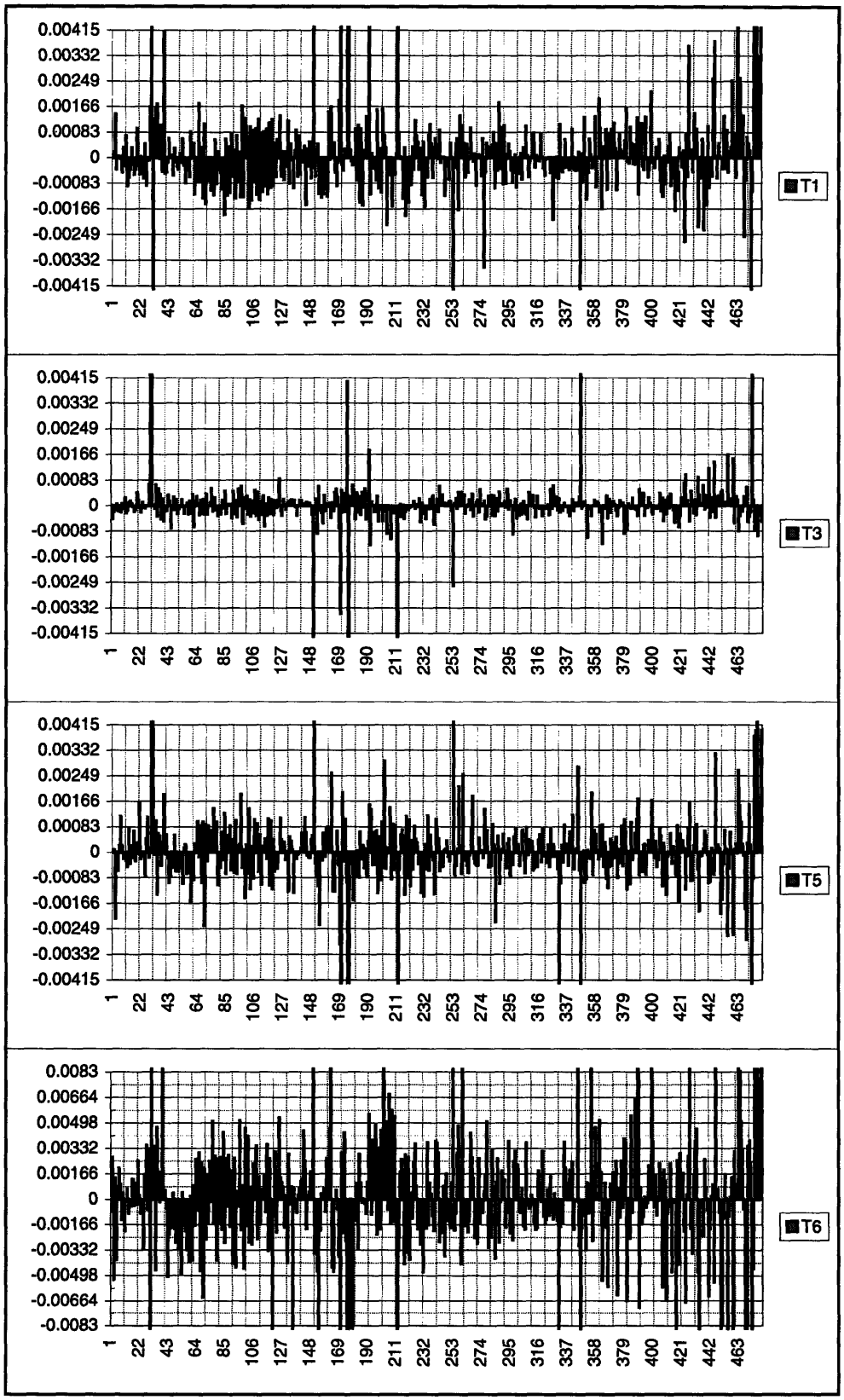

Figure A-4: PCU results for all 6 temperatures on FPA 29 [Test ID: 181807b].

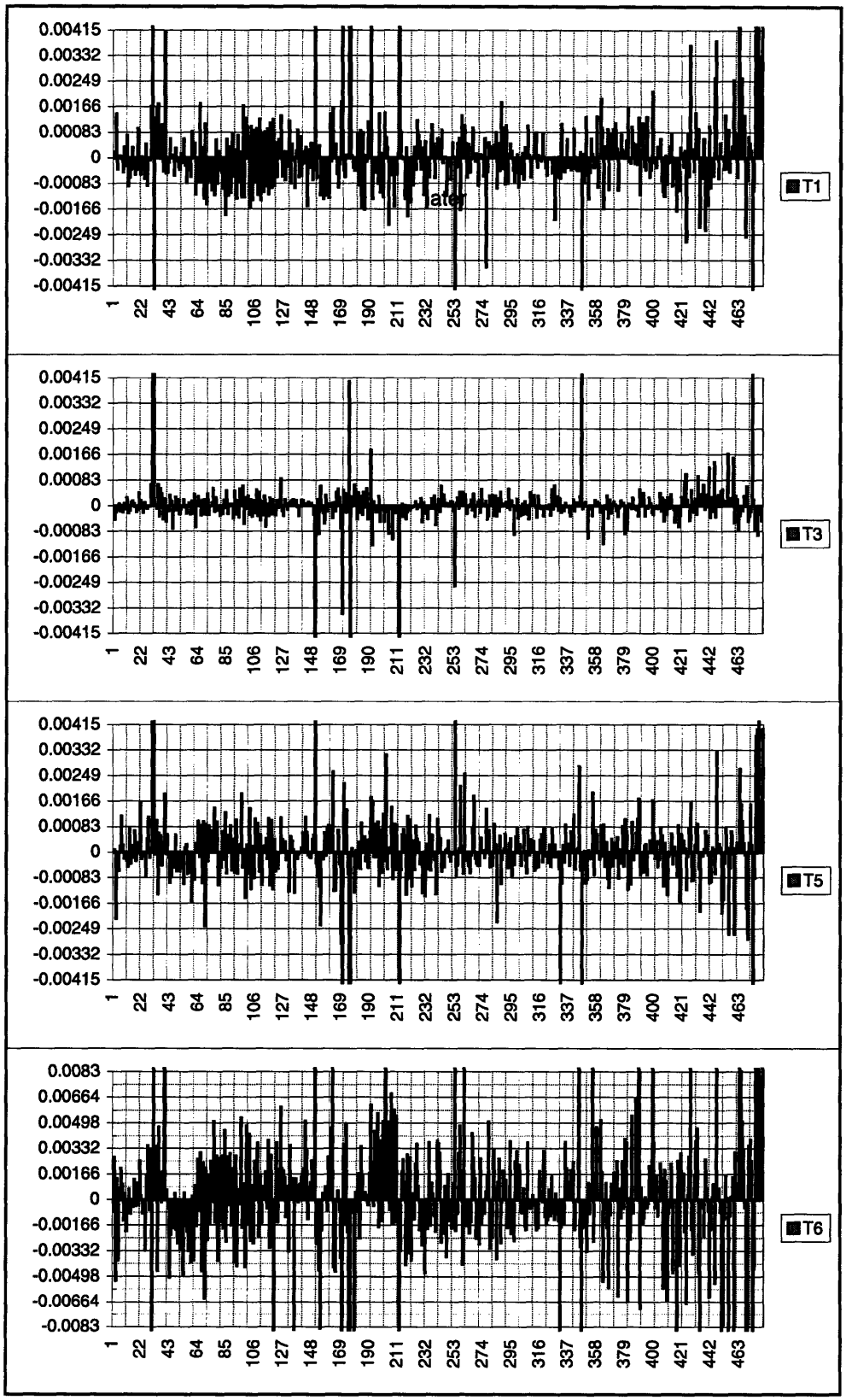

Figure A-5: PCU results for all 6 temperatures on FPA 29 [Test ID: 182109b].

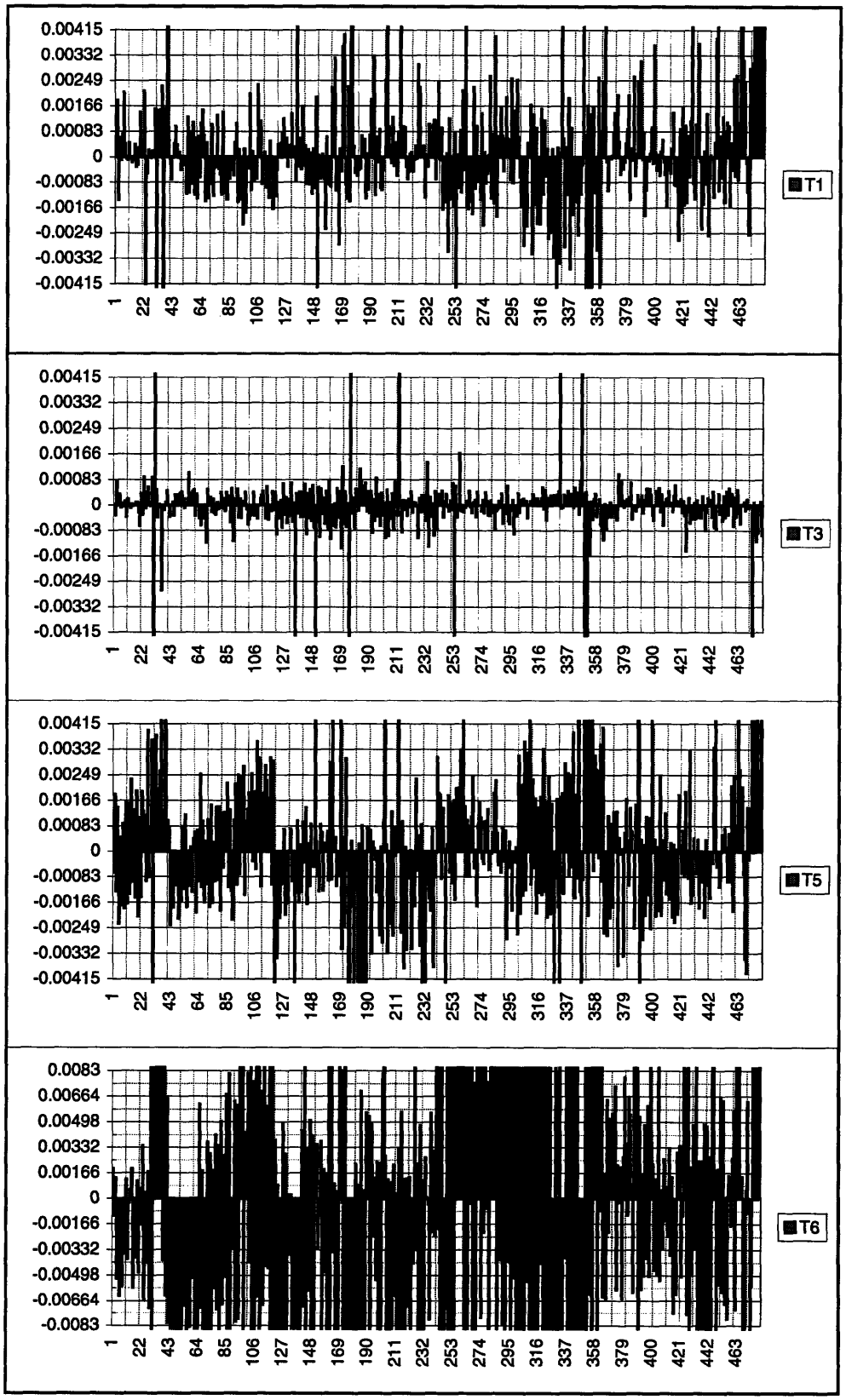

Figure A-6: PCU results for all 6 temperatures on FPA 29 [Test ID: 191724].

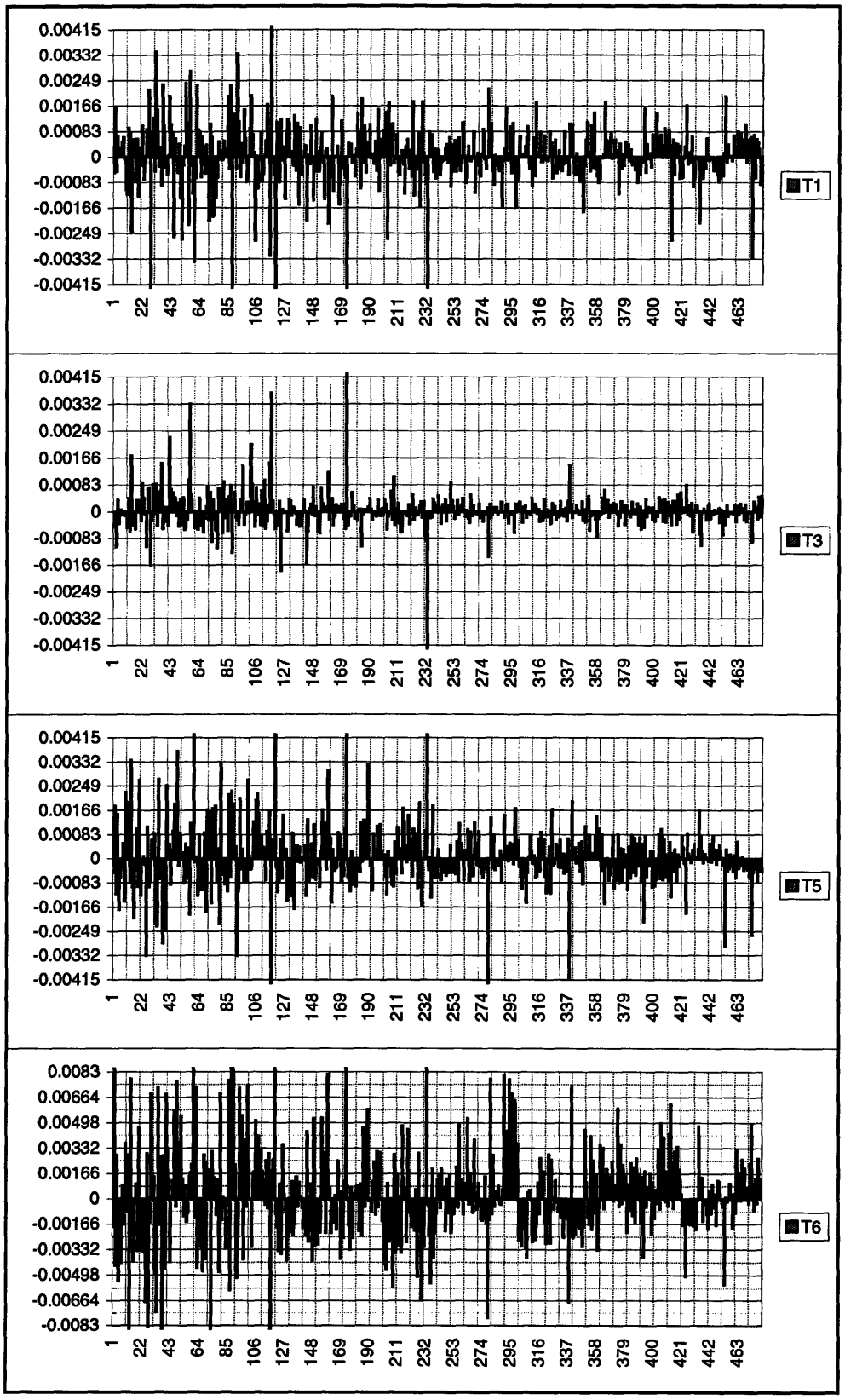

Figure A-7: PCU results for all 6 temperatures on FPA 32 [Test ID: 151830a].

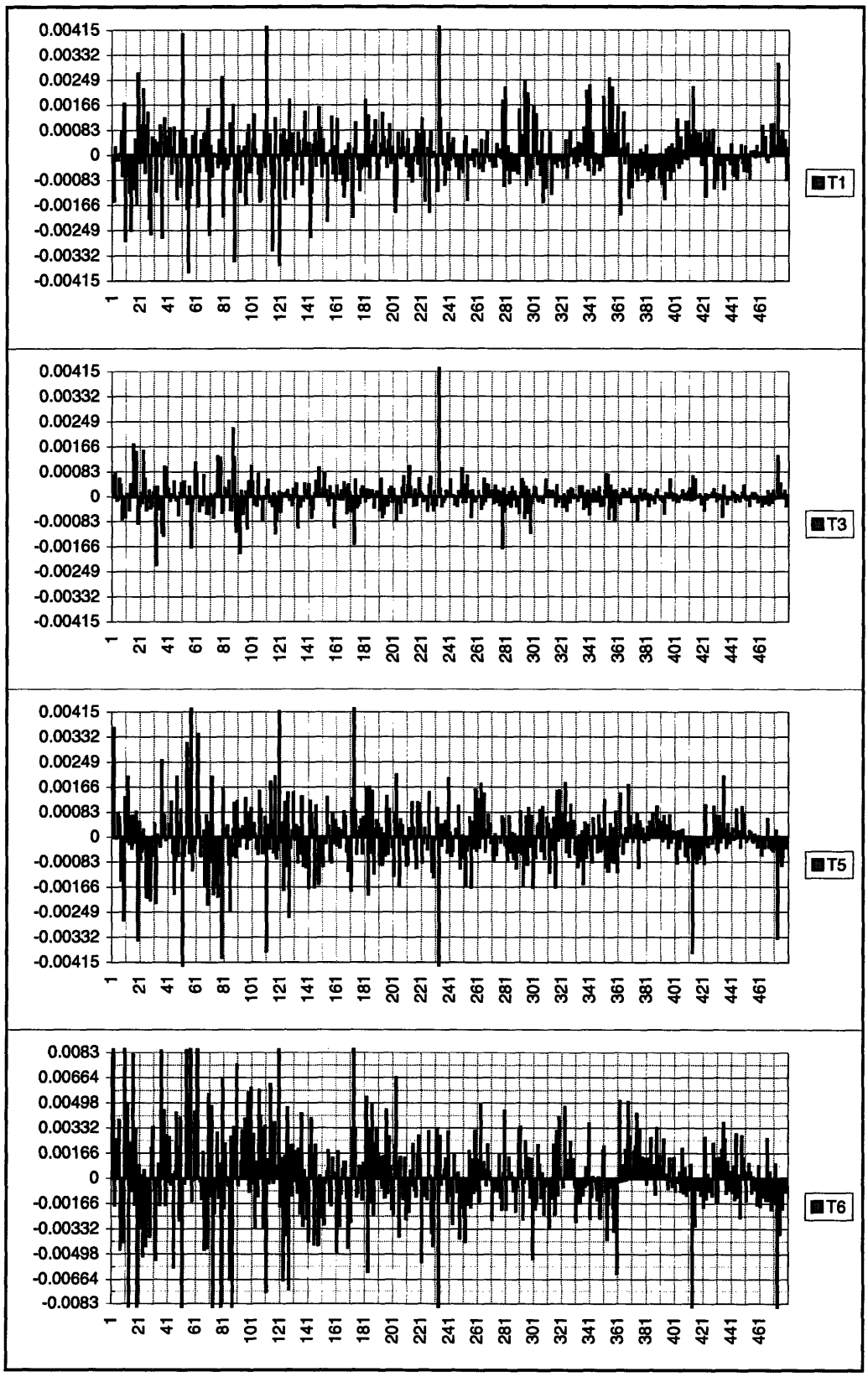

Figure A-8: PCU results for all 6 temperatures on FPA 32 [Test ID: 151830b].

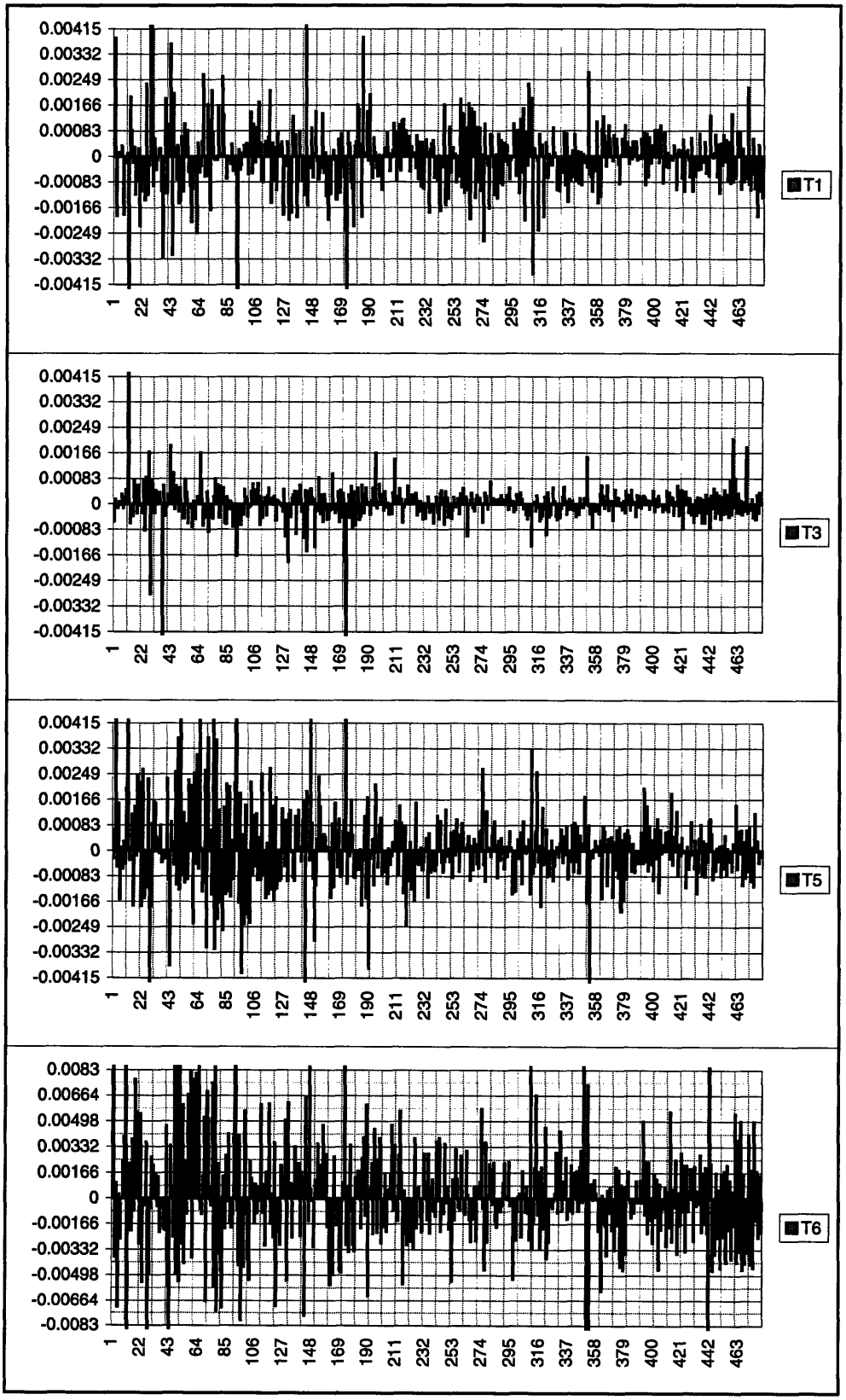

Figure A-9: PCU results for all 6 temperatures on FPA 32 [Test ID: 212336a].

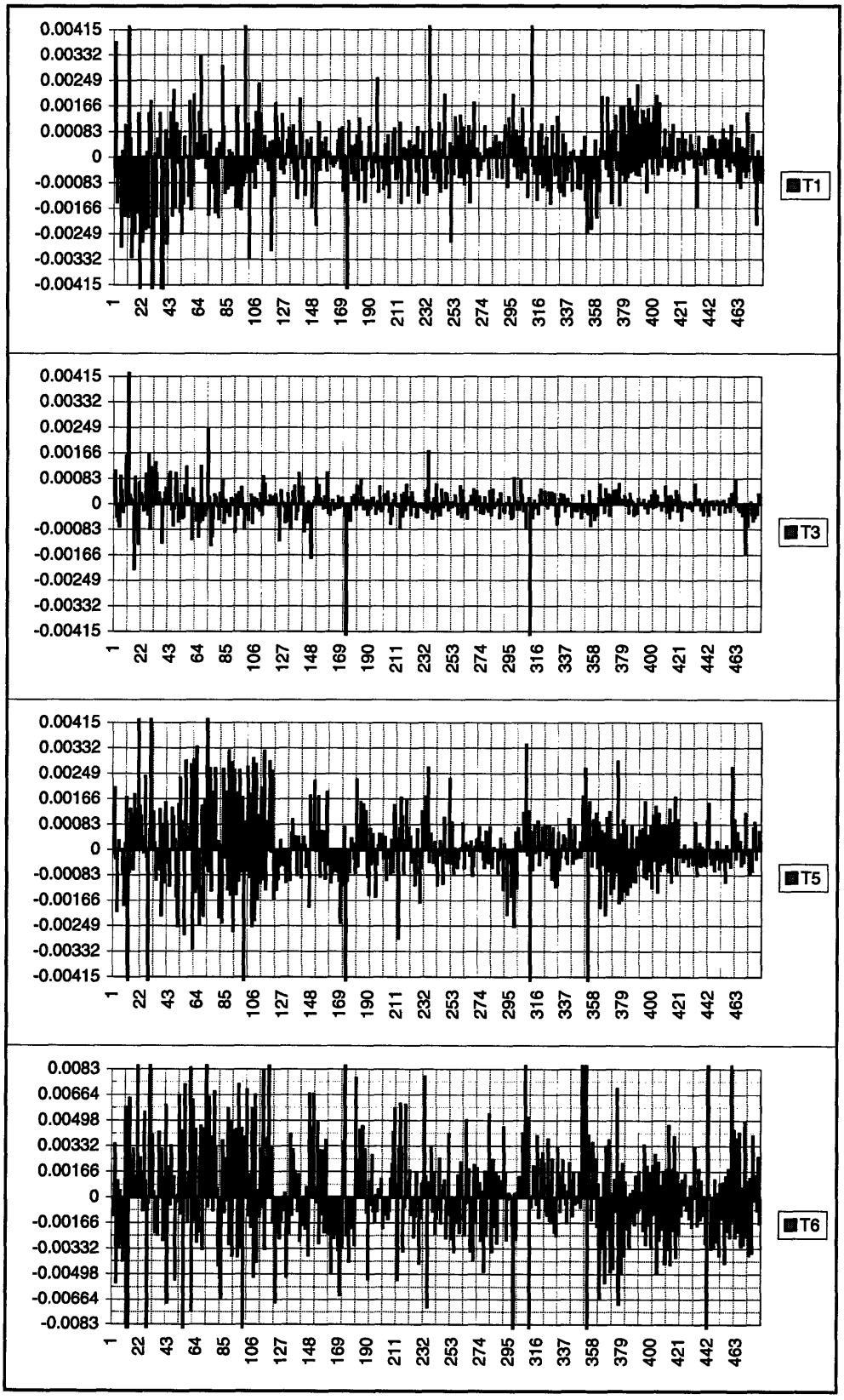

Figure A-10: PCU results for all 6 temperatures on FPA 32 [Test ID: 212336b].

Bibliography

[1] A. Darryl Adams, Greg Johnson, Noel D. Jolivet, and Jeff Metschuleit. Optimizing scanning array performance using gain normalization and time delay and integrate (TDI) pixel deselection during readout, hybrid and focal plane testing. volume 1686. SPIE, 1992.

[2] Paul A. Bell, Stanley J. Pruchnic, Jr., and Edward M. Lewis. Evaluation of temporal stability and spatial uniformity of blackbody thermal reference sources. volume 2470. SPIE, 1994.

[3] P. R. Bevington. *Data Reduction and Error Analysis for the Physical Sciences.* McGraw Hill Book Co., New York, 1969.

[4] Glenn D. Boreman and Christopher Costanzo. Compensation for gain nonuniformity and nonlinearity in HgCdTe infrared charge-couple-device focal planes. *Optical Engineering*, 26(10):981–984, October 1987.

[5] Vikram Dhar and R. Ashokan. Computer simulation of fixed-pattern-noise-limited noise-equivalent-temperature differences in mercury cadmium telluride focal-plane arrays. *Optical Engineering*, 34(5):1316–1324, May 1995.

[6] W. R. Herzog and K. Williams. Fixed pattern noise in night vision systems – linearity/uniformity/correctability. Analysis Report ANA21020000-005, Martin Marietta Technologies Inc., Orlando, FL, October 1994.

[7] James P. Karins. Models of nonlinearities in focal plane arrays. In *Infrared Detectors and Focal Plane Arrays II*, volume 1685, pages 103–109. SPIE, 1992.

[8] Daniel P. Lacroix and James Wey. SADA II 1-clip 480x6 TDI ROIC design report. Design Report #21034478, Loral Infrared and Imaging Systems, Lexington, MA, June 1995.

[9] Kevin Maschhoff. FPA/Dewar requirements on spectral response uniformity related to image uniformity-after-correction performance. Interoffice correspondence, Lockheed Martin IR and Imaging Systems, July 1996.

[10] A. F. Milton, F. R. Barone, and M. R. Kruer. Influence of nonuniformity on infrared focal plane array performance. *Optical Engineering*, 24(5):855–862, September/October 1985.

[11] Jonathan M. Mooney, Freeman D. Shepherd, William S. Ewing, James E. Murguia, and Jerry Silverman. Responsivity nonuniformity limited performance of infrared staring cameras. *Optical Engineering*, 28(11):1151–1161, November 1989.

[12] Paul Norton and William Radford. Responsivity uniformity of infrared detector arrays. *Semicond. Sci. Technol.*, 6:C96–C98, 1991.

[13] John J. O'Neill, III, Christopher Costanzo, and David Kaplan. Characterization of post correction uniformity on infrared focal plane arrays. volume 2474. SPIE, 1995.

[14] David L. Perry and Eustace L. Dereniak. Linear theory of nonuniformity correction in infrared staring sensors. *Optical Engineering*, 32(8):1854–1859, August 1993.

[15] George V. Poropat. Nonlinear compensation for responsivity nonuniformities in cadmium mercury telluride focal plane detector arrays for use in the 8 to 12 μm spectral region. *Optical Engineering*, 28(8):887–896, August 1989.

[16] M. Schulz and L. Caldwell. Nonuniformity correction and correctability of infrared focal plane arrays. volume 2470, pages 200–211. SPIE, 1995.

[17] Dean A. Scribner, M. R. Kruer, C. J. Gridley, and K. A. Sarkady. Physical limitations to nonuniformity correction in IR focal plane arrays. In *Focal Plane Arrays: Technology and Applications*, volume 865, pages 185–202. SPIE, 1987.

[18] Dean A. Scribner, K. A. Sarkady, M. R. Kruer, and C. J. Gridley. Test and evaluation of stability in IR staring focal plane arrays after nonuniformity correction. In *Test and Evaluation of Infrared Detectors and Arrays*, volume 1108, pages 255–264. SPIE, 1989.

[19] John R. Taylor. *An Introduction to Error Analysis: The Study of Uncertainties in Physical Measurements.* Oxford University Press, 1982.

[20] Development specification for non-optical improvement standard advanced dewar assembly, type two (SADA-II, NON-OI). Development Specification B2-A3190640B, May 1995. Includes changes described in approved Engineering Change Proposal (ECP No. J504-001) of Feb. 22, 1996.